Carbon 244 (2025) 120658

Contents lists available at ScienceDirect

Carbon

journal homepage: www.elsevier.com/locate/carbon

Evolution and mechanism of frictional properties of DLC coatings and iron surfaces under hydrogen-atom irradiation

Hu Zhang [a], Shu Xiao [a,*], Yong Huang [a], Qingdong Ruan [a], Guohua Chen [a], Saihua Jiang [a], Chao Yang [b,**], Paul K. Chu [c]

[a] School of Mechanical & Automotive Engineering, South China University of Technology, Guangzhou, 510641, China
[b] National Engineering Research Center of Light Alloy Net Forming, School of Materials Science and Engineering, Shanghai Jiao Tong University, Shanghai, 200240, China
[c] Department of Physics, Department of Materials Science and Engineering, and Department of Biomedical Engineering, City University of Hong Kong, Tat Chee Avenue, Kowloon, Hong Kong, China

ARTICLE INFO

Keywords:
H-atom irradiation
Hydrogen permeation barrier
DLC
Friction
Molecular dynamics simulation

ABSTRACT

DLC coatings have great potential in semiconductor manufacturing due to their excellent friction and hydrogen permeation barrier (HPB) properties. However, how H-atom irradiation affects interfacial structure evolution and friction remains unclear, largely due to the limitations of in situ characterization techniques. This study combines molecular dynamics simulations and experiments to investigate the effects of H-atom irradiation on the interfacial structure and frictional properties of Fe substrate/DLC coatings. The hydrogen permeability of DLC is approximately three orders of magnitude lower than that of the Fe substrate ($\sim 10^3$), indicating superior hydrogen resistance. H-atom irradiation degrades the friction of the Fe substrate by producing lattice phase transitions and interfacial defects. In contrast, H-atom irradiation enhances the structural order of the DLC coating by modifying the carbon bonding at the interface, improving strain distribution, and reducing local stress concentrations. This strain control improves the durability of the graphene-like six-membered ring structure formed at the friction interface, thus enhancing the DLC friction performance under H-atom irradiation. This study elucidates the atomic-scale mechanisms for hydrogen-induced structural evolution and enhancement of frictional properties in DLC coatings and offers insights into their applications to semiconductor manufacturing.

1. Introduction

Hydrogen plasma is an ionized gas consisting of positively charged hydrogen ions (H^+), electrons (e^-), neutral hydrogen atoms (H), hydrogen molecules (H_2), and energetic particles. It is widely used in the etching of thin films as well as cleaning and modification of surfaces [1]. As a core process medium for semiconductor manufacturing, its highly reactive particle environment induces severe surface degradation on precision components (such as slide rails), which will affect its friction performance [2–4]. Continuous hydrogen permeation into steel substrates triggers hydrogen embrittlement, resulting in microcrack initiation and mechanical property deterioration, which has emerged as a critical bottleneck in limiting the service lifetime of semiconductor equipment [5]. Owing to their exceptionally small atomic radius, hydrogen atoms preferentially diffuse along defect pathways including grain boundaries and dislocations, causing a synergistic deterioration of both strength and toughness in structural materials [6–9]. Therefore, developing lubricant coatings with hydrogen embrittlement and corrosion resistance is crucial to addressing wear failure in hydrogen plasmas.

Diamond-like carbon (DLC) coatings have significant potential as wear-resistant coatings on precision components in semiconductor equipment because of low friction, superior wear resistance, high hardness, and excellent chemical inertness [10–12]. High-density DLC coatings are also effective hydrogen barriers [13–15]. Abbas et al. [16] have studied the gas barrier properties of DLC coatings. Owing to the amorphous structure of DLC coatings, the nanopores in the films serve as 'hydrogen traps' to reduce hydrogen permeation [17–19]. Tamura et al. [20] have discovered that DLC coatings with a high concentration of hydrogen have high hydrogen permeability resistance because hydrogen influences the bonding state of carbon and alters the density and

* Corresponding author.
** Corresponding author.
E-mail addresses: xiaos@scut.edu.cn (S. Xiao), chaoyang0315@163.com (C. Yang).

https://doi.org/10.1016/j.carbon.2025.120658
Received 16 May 2025; Received in revised form 21 July 2025; Accepted 23 July 2025
Available online 23 July 2025

hardness of the materials. At low hydrogen content, the density and hardness of the coating increase, leading to improved wear resistance. Conversely, if the hydrogen concentration is large, 'hydrogen traps' can be occupied by hydrogen atoms to block the diffusion of hydrogen through the coatings. However, due to constraints in temporal and spatial resolution, most studies have primarily focused on experimental observations. Consequently, it is important to gain a better understanding of the structural evolution and underlying mechanism of DLC coatings during exposure to hydrogen plasmas.

Molecular dynamics (MD) simulation is a powerful method that can overcome the limitations of spatial and temporal resolution in experimental research. Due to its unique in-situ observation advantages, it has become a popular tool for studying the mechanisms of diamond-like carbon (DLC) coatings [21–26]. For instance, Shi et al. [23] have studied the effects of the C-atom irradiation dose on the mechanical properties of amorphous carbon (a-C) films and determined the intrinsic relationship between structural changes and materials properties. In another study, Shi et al. [24] have explored the interactions and mechanism of atomic oxygen (AO) irradiation on amorphous carbon and the direct correlation between the interfacial atom removal and interfacial bonding energy. However, research on hydrogen irradiation effects in diamond-like carbon (DLC) coatings remains scarce, with existing studies predominantly addressing carbon, oxygen, and swift heavy ion irradiation [25].

Owing to the limitations in temporal and spatial resolution of conventional experimental approaches, the underlying mechanisms governing irradiation-induced structural evolution in thin films remain incompletely understood. Moreover, a comprehensive assessment of the mechanical properties (especially tribological properties) of irradiated films is particularly lacking. To address the aforementioned limitations, molecular dynamics (MD) simulations are performed to systematically investigate the effects of H-atom irradiation on the interfacial structural evolution of the Fe substrate/DLC coating system. The diffusion behavior of hydrogen atoms and the influence on the tribological properties are investigated. The simulation results, validated with experimental data, demonstrate excellent accuracy and reliability. This study not only provides fundamental insights into the irradiation-induced structural evolution of DLC coatings, but also lays a scientific foundation for facilitating their application in addressing key friction and wear challenges in the semiconductor industry.

2. Computational methods and experimental details

2.1. Molecular dynamics calculations

The diffusion behavior of hydrogen atoms at the interface between the Fe substrate and DLC coating was investigated using the large-scale atomic/molecular massively parallel simulator (LAMMPS) [27], and the effects of hydrogen irradiation on the friction properties were determined. The simulation results were visualized using the open visualization tool (OVITO) [28]. To facilitate the discussion and differentiation of the samples under various conditions, the following nomenclature was adopted in this study: *Fe* denoting the pure Fe substrate without irradiation, *H_Fe* denoting the Fe substrate irradiated with hydrogen atoms, *DLC* denoting the diamond-like carbon coating without irradiation, and *H_DLC* denoting the diamond-like carbon coating irradiated with hydrogen atoms. The simulations were carried out using the following interatomic potentials. The adaptive intermolecular reactive empirical bond order (AIREBO) potential, which described C–C, C–H, and H–H interactions in DLC coatings, was adopted to simulate the chemical reactions and intermolecular interactions in amorphous carbon systems [29]. The Tersoff potential described the C–C interactions in the frictional counterpart of diamond [30]. The embedded atom method (EAM) potential described Fe–Fe, Fe–H, and H–H interactions [31], and the Lennard-Jones (L-J) potential function was used to describe the interactions between frictional counterparts, DLC coatings, Fe substrates, and hydrogen atoms. The interaction parameters for the L-J potential function are listed in Table 1 [32,33].

The simulation system consisted of the Fe substrate and DLC coating with dimensions of 90 Å × 90 Å × 45 Å. To mitigate boundary effects [34,35], periodic boundary conditions were applied in the X- and Y-directions, while free boundary conditions were applied in the Z-direction. The Fe substrate was modeled as a body-centered cubic (BCC) lattice containing 30799 Fe atoms. The DLC coating, comprising 46552 C atoms, was constructed by the 'liquid quenching' method, which had been demonstrated to accurately reproduce the properties of DLC coatings in experimental studies [36–38]. The construction process involved four steps: melting, constant temperature, quenching, and relaxation. Initially, a crystalline diamond block was heated rapidly to 8300 K at a rate of 1000 K/ps. The system was maintained at 8300 K for 10 ps to achieve temperature equilibration and then quenched to 300 K at a rate of 1000 K/ps. Finally, to eliminate residual stresses, the system was relaxed for 30 ps using the NPT ensemble at 300 K. The resulting DLC model had a density of 2.6 g/cm^3 [39].

In the H-atom irradiation simulation, atoms in the 0–5 Å region at the bottom of the model were fixed to ensure structural stability during irradiation. The 5–15 Å region was designated as the thermostatic layer, and its temperature was maintained at 300 K by a Langevin thermostat. The 15–45 Å region was designated as the Newton layer. Prior to irradiation, structural relaxation was performed to the DLC layer at 300 K to produce the optimal atomic configuration and energy minimization. During irradiation, hydrogen atoms were directed toward the model surface with an initial kinetic energy of 100 eV from a 90 Å × 90 Å irradiation region positioned at 45 Å above the surface. The choice of hydrogen atoms (rather than hydrogen ions) as incident particles was based on the following rationale. At low kinetic energies, energy transfer is predominantly governed by nuclear collision processes, and the contribution of electron interactions can be neglected [40]. The irradiation time interval was set to 2 ps to ensure the complete interaction between each hydrogen atom and surface. Fig. S1 illustrates the temporal evolution of kinetic energy, potential energy, total energy, and interfacial temperature as functions of irradiation time. A total of 200 hydrogen atoms were irradiated using a time step of 0.1 fs/step. The irradiation process is illustrated in Fig. 1a. To characterize the motion state of hydrogen atoms in the model after irradiation and their influence on the evolution of the bonding structure, a 100 ps dynamic simulation was performed for the irradiated model. The mean square displacement (MSD) of hydrogen atoms, the "hydrogen diffusion coefficient" and the spatial non-uniformity (h) of carbon atom distribution were calculated. The MSD was calculated as follows [41]:

$$MSD(t) = r^2(t) = \frac{1}{N}\sum_{i=1}^{N} |r_i(t) - r_i(0)|^2 \quad (1)$$

where N is the number of i atoms in the system and $r_i(t)$ and $r_i(0)$ are the positions of the i_{th} atom at time t and 0, respectively. The calculation method for the "hydrogen diffusion coefficient" is shown in Eq. (2).

$$D = \lim_{t\to\infty} \frac{1}{6N}\sum_{i=1}^{N} |r_i(t) - r_i(0)|^2 \quad (2)$$

The coefficient before the MSD takes the value of 1/6 for a three-dimensional system. The expression for the spatial non-uniformity (h) of the carbon atom distribution is shown in Eq. (3) [42]:

Table 1
Lennard-Jones energies (ε) and distances (Å) for C, Fe and H.

Species	ε (eV)	σ (Å)
C–C	0.00284	3.4
C–H	0.00207	3.025
C–Fe	0.02495	3.7

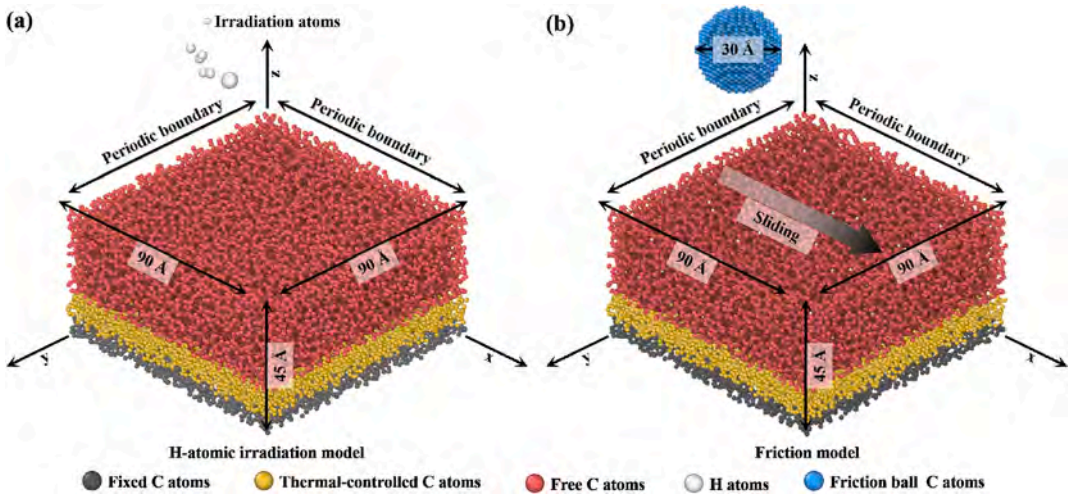

Fig. 1. Simulation process: (a) Schematic of the MD model for H-atom irradiation of DLC films, (b) Schematic of the MD model for friction between the diamond frictional counterpart and hydrogen atom irradiated DLC films.

$$h=\frac{1}{2N}\sum_{k=1}^{r}8.89^{1-k}\sum_{i=1}^{2^{3k}}\left|m_i-\overline{m}\left(2^{3k}\right)\right| \tag{3}$$

where h is the local inhomogeneity parameter. The closer the value to 1, the more the atoms are clustered together. N represents the number of atoms, r is the smallest integer that satisfies $2^{3k} > N$, m_i is the number of atoms contained in each grid element, and $\overline{m}$ is the average of m_i.

In the friction simulation, the fixed layer, thermostatic layer, and Newton layer of the model were consistent with those used in the irradiation simulation, as shown in Fig. 1b. A frictional counterpart composed of diamond atoms with a radius of 15 Å was utilized. To prevent the deformation of the diamond frictional counterpart under load and friction, it was defined as a rigid body. The time step was set to 0.5 fs/step. The simulation was divided into three stages: relaxation, loading, and friction. In the relaxation stage, to ensure no initial interaction between the model and the diamond frictional counterpart, the frictional counterpart was positioned 20 Å above the model surface along the Z-axis. The system was relaxed for 10 ps to achieve a steady state and eliminate residual stresses from the initial structure. In the loading stage, the diamond frictional counterpart was moved along the Z-axis at a speed of 0.2 Å/ps until a predetermined loading depth of 5 Å was reached. In the friction stage, at a sliding speed of 0.2 Å/ps, the diamond frictional counterpart was moved horizontally along the X-axis. The frictional counterpart slid out of the model from its initial position, re-entered from the same position, and completed five friction cycles. The friction process is illustrated in Fig. 1b. In order to characterize the distribution of interface stress during the friction process, the hydrostatic stress and Von-Mises stress of the friction interface were calculated. The calculation of hydrostatic stress and Von-Mises stress is as follows [43,44]:

$$\sigma_{\mathrm{Hyd}}=\frac{1}{3}\left(\sigma_1+\sigma_2+\sigma_3\right) \tag{4}$$

$$\sigma_{\mathrm{von}}=\sqrt{3\left(\sigma_{12}^2+\sigma_{13}^2+\sigma_{23}^2\right)+\frac{1}{2}\left[\left(\sigma_1-\sigma_2\right)^2+\left(\sigma_2-\sigma_3\right)^2+\left(\sigma_3-\sigma_1\right)^2\right]} \tag{5}$$

where σ_{11}, σ_{22}, σ_{33}, σ_{12}, σ_{13} and σ_{23} are the stress compo nents of atoms in the Newtonian layer. The calculating of wear rate is as follows [45,46]:

$$K=\frac{V}{F\times S} \tag{6}$$

where V is the total loss volume ($Å^3$) of the film caused by wear, F is the contact force, and S is the total friction distance (Å).

2.2. Materials preparation, tribological assessment, and characterization

The substrate for DLC deposition was X70 industrial pipeline steel with dimensions of 50 × 30 × 1.5 mm. Prior to deposition, the substrate was cleaned ultrasonically in deionized water and anhydrous ethanol. The DLC coating was fabricated in a DC magnetron sputtering system. Initially, the sample was positioned in a vacuum chamber evacuated to a base pressure of 1×10^{-3} Pa, followed by the introduction of high-purity Ar (99.9995 %) to reach a working pressure of 0.4 Pa. Surface pretreatment was performed by applying 1000 V to a linear ion source, and Ar plasma cleaning was conducted for 30 min to activate the surface. To enhance interfacial adhesion, a Ti interlayer was deposited by sputtering of a high-purity Ti target (99.9 %) for 20 min at −100 V using a pulsed DC power supply (500 W). Subsequently, a Ti–C gradient transition layer was synthesized by co-sputtering of C (99.9 %) and Ti targets. The Ti target power was reduced linearly from 500 W to 0 W while the C target power increased from 0 W to 500 W during the 30-min deposition period. Finally, the DLC film was deposited for 120 min at a constant bias voltage with the C target maintained at 500 W. The experimental parameters are presented in Table 2.

In the hydrogen plasma treatment, both the uncoated and diamond-like carbon (DLC)-coated specimens were positioned in a vacuum chamber for plasma irradiation. Prior to treatment, the chamber was evacuated to a base pressure of 1.5×10^{-3} Pa using a turbomolecular pump. A gas mixture of argon and hydrogen (5 % H_2) was subsequently introduced through a mass flow controller at 20 standard cubic centimeters per minute (sccm), establishing a working pressure of 0.15 Pa. Plasma generation was achieved using a linear ion source powered by a pulsed DC supply operating in constant-voltage mode (1200 V, 0.05 A), delivering an effective power of 60 W. The substrate holder was maintained at a negative DC bias of −100 V to optimize ion flux

Table 2
Experimental parameters of DLC deposition.

Step	Ti target power (W)	C target Power (W)	Substrate bias voltage (V)	Time (min)
Ion cleaning	0	0	−100	30
Ti layer	500	0	−100	20
Gradient layer	500 → 0	0 → 500	−100	30
Carbon layer	0	500	−100	120

directionality, and the hydrogen plasma irradiation lasted for 60 min. During the experiment, due to the thermal effect of the plasma, the temperature of the chamber increased by about 5 K. The sample was removed by cooling after irradiation.

Field-emission scanning electron microscopy (FE-SEM, SU8600) was performed at 5 kV to examine both the surface and cross-sectional morphologies of the unirradiated and H-atom irradiated DLC coatings. Laser confocal micro-Raman spectrometry (HJY LabRAM Odyssey) was employed to monitor the structural evolution of DLC coatings during H-atom irradiation and friction processes. X-ray photoelectron spectroscopy (XPS, Kratos Axis Supra^{+}, UK) was utilized to determine the chemical composition of the coatings before and after the tribological test. The tribological properties were determined on a ball-on-disc tribometer (MS ETC3000) with GCr15 steel balls (Ø = 6 mm) as counterparts under the following conditions: 5 N normal load, 200 rpm rotational speed, 5 mm wear track radius, and 30-min test duration. The wear track morphology was quantitatively analyzed by 3D optical profilometry (Talysurf CLI 1000).

3. Results and discussion

3.1. Irradiation-induced interfacial microstructural modification

H-atom irradiation forms vacancy defects on the Fe surface, as shown in Fig. 2a. Hydrogen atoms predominantly occupy the interstitial sites in the Fe substrate lattice. The phenomenon is attributed to vacancy occupation facilitated by the inherent interstitial structure of the Fe lattice coupled with the small atomic radius and high chemical reactivity of hydrogen [5]. Analysis of hydrogen atom trajectories in the Fe substrate (Fig. 2c1) reveals irregular diffusion patterns through lattice gaps [47,48]. The drawing of a schematic diagram of the diffusion motion of H atoms in the Fe matrix is based on this, as shown in Fig. 2c2. Computational analysis of the lattice structure evolution and interface dislocation (Fig. 2c3-c4) demonstrates that hydrogen spurs the BCC phase transformation, which increases with hydrogen concentration. The interaction between hydrogen atoms and dislocations exhibits a complex dual nature (Fig. S2), while increasing the hydrogen concentration reduces the dislocation diffusion energy and enhances dislocation mobility [48–50]. Hydrogen atoms also exhibit the tendency to accumulate at and pin pre-existing interfacial dislocations, thereby restricting their movement [51–53].

In contrast, when diffusing hydrogen atoms encounter dangling carbon bonds in or on the DLC coating, they form stable C–H bonds, a critical mechanism contributing to the hydrogen barrier properties [54, 55]. The amorphous DLC coatings have numerous irregular nanopores [56]. When hydrogen atoms diffuse to these nanopores (Fig. 2d3), they maintain the high energy states due to the absence of stable chemical bonding. Notably, despite the lack of strong chemical interactions, hydrogen diffusion remains constrained (Fig. 2d3) as surrounding carbon atoms create a weak van der Waals interaction barrier [20]. This nanopore confinement mechanism, mediated by van der Waals forces, impedes hydrogen atom diffusion in the DLC coating.

Based on dynamic simulation results of the H-atom irradiation model, the hydrogen diffusion behavior of the Fe substrate and DLC coating was compared (Fig. 3a–b). The distribution and clearer migration paths of hydrogen atoms (disregard of DLC or Fe morphology) are shown in Fig. S3. The results reveal distinct diffusion characteristics: the Fe substrate facilitates irregular hydrogen atom diffusion primarily through lattice gaps, while the DLC coating shows substantial hydrogen atom diffusion inhibition. Mean square displacement (MSD) calculations

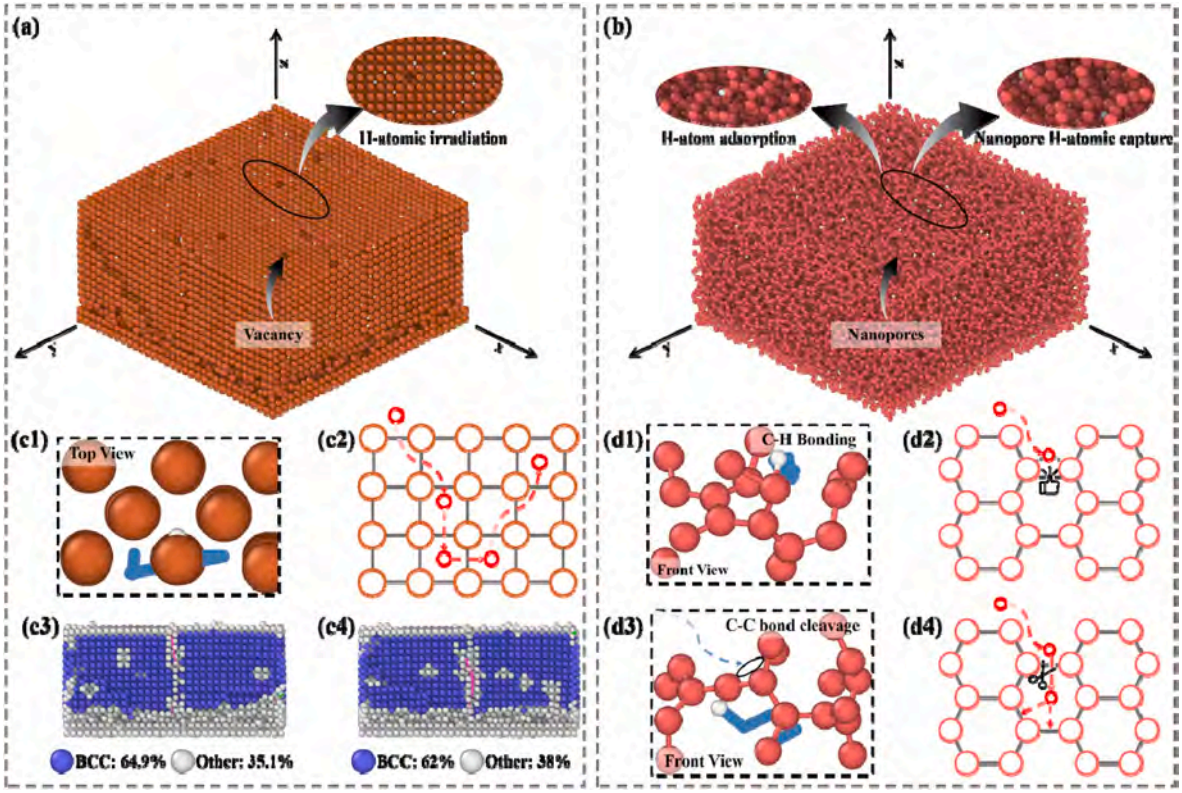

Fig. 2. Morphological evolution and atomic-scale mechanisms of H-atom irradiated effects: (a) Surface morphological alterations of Fe substrate induced by H-atom irradiation; (b) Structural modifications of DLC layer following H-atom irradiation; (c1) Three-dimensional trajectory mapping of hydrogen atoms within Fe substrate (The blue line is the atomic motion trajectory); (c2) Enhanced trajectory visualization of hydrogen atoms on Fe substrate surface; (c3-c4) Atomic structure and dislocation changes in Fe substrate during H-atom irradiation; (d1, d3) Magnified trajectory visualization of hydrogen atoms within DLC layer (The blue line is the atomic motion trajectory.); (d2, d4) Three-dimensional trajectory mapping of hydrogen atoms diffusion in DLC layer. (For interpretation of the references to color in this figure legend, the reader is referred to the Web version of this article.)

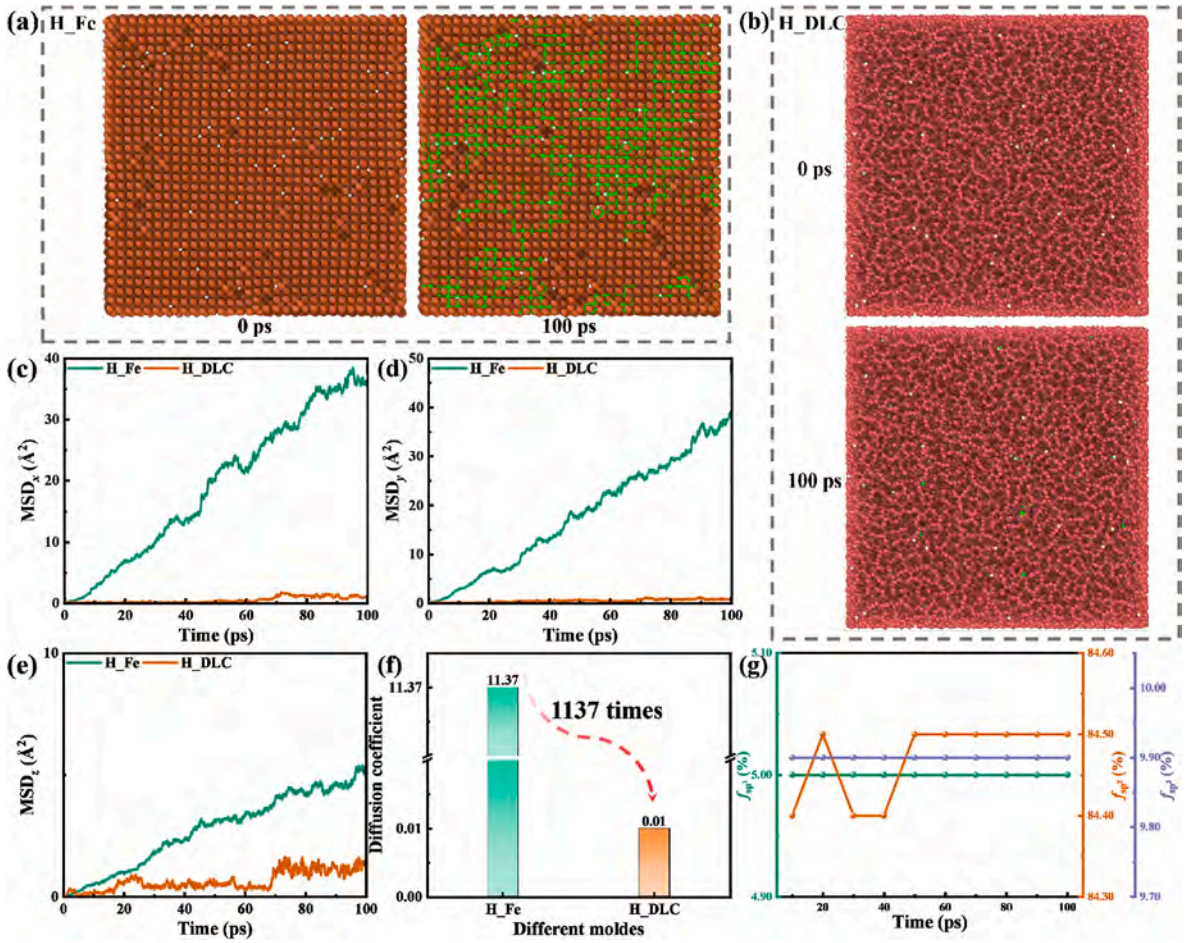

Fig. 3. Dynamic simulation analysis of the H-atom irradiation behavior: (a) Trajectory mapping of hydrogen atom diffusion on the Fe substrate surface (The green line is the atomic motion trajectory.); (b) Hydrogen atom diffusion pathway on the DLC coating surface (The green line is the atomic motion trajectory.); (c–e) Mean square displacement (MSD) profiles of irradiated hydrogen atoms along the x-, y-, and z-axes; (f) Comparative analysis of hydrogen atom diffusion coefficients in different materials; (g) Evolution of the hybrid bond content in DLC coating during H-atom irradiation. (For interpretation of the references to color in this figure legend, the reader is referred to the Web version of this article.)

of irradiated hydrogen atoms indicate greater diffusion tendencies along the X, Y, and Z directions in the Fe substrate compared to the DLC coating (Fig. 3c–e). These findings suggest that while the Fe substrate supplies relatively unimpeded hydrogen atom diffusion pathways, the DLC coating restricts hydrogen atom diffusion [14]. Quantitative analysis of the diffusion coefficients substantiates the observations, revealing that the hydrogen diffusion coefficient in DLC is 1/1137 of that in the Fe substrate (Fig. 3f). The results are in agreement with previous findings [20]. Kinetic analysis reveals that the hybrid bonding structure at the DLC interface exhibits remarkable stability, demonstrating that hydrogen atom diffusion within the coating does not considerably modify its structural configuration (Fig. 3g).

3.2. Irradiation-induced alterations of interfacial friction properties

By performing a comprehensive analysis of H-atom irradiation, the lattice structure of the Fe substrate facilitates hydrogen atom diffusion and H-atom irradiated surface defect formation, as shown in Figs. 2 and 3. In contrast, the DLC coating shows effective hydrogen adsorption and retention without altering the hybrid bonding structure. The tribological properties, which are crucial to the stable operation of semiconductor manufacturing equipment, are assessed by evaluating the irradiation-induced changes in the friction properties. Particularly, hydrogen-induced surface modification of the Fe substrate and the hydrogen adsorption characteristics of the DLC coating may influence the tribological properties upon irradiation. Furthermore, irradiation-induced surface defects, dislocation slips, and hydrogen adsorption may evolve during friction to potentially alter the tribological response. Therefore, the friction behavior of the non-irradiated and H-atom irradiation systems is determined to assess the irradiation effects on wear properties of both the Fe substrate and DLC coating.

Fig. 4 displays the simulated results during friction. Fig. 4a presents the friction curves of the four systems for five friction cycles (The load variation during friction is shown in Fig. S4.). In the initial stage (0–90 Å, first cycle), the friction decreases in the following order: H_Fe > Fe > DLC > H_DLC. The reduced friction of H_DLC may be attributed to surface reconstruction resulting from H-atom irradiation, which also decreases the contact resistance [36]. Notably, both the Fe and H_Fe systems exhibit significant friction fluctuations, showing an initial increase and then a gradual decrease, resulting from substantial contact stress and interfacial plastic deformation in the early stage, followed by stress relaxation as friction progresses. The friction coefficient curves in Fig. 4b reveal that both DLC systems have superior tribological properties, with H_DLC showing enhanced stability throughout the test. However, H_Fe shows a larger friction coefficient, indicating the detrimental effects of H-atom irradiation on the Fe substrate tribological properties. Furthermore, as shown in Fig. 4c, the average frictional force and coefficient of the system with the frictional force and coefficient of the four models in the 3rd to 5th cycles are calculated. The DLC system maintains an average friction force of 6.63 nN and a coefficient of 0.04.

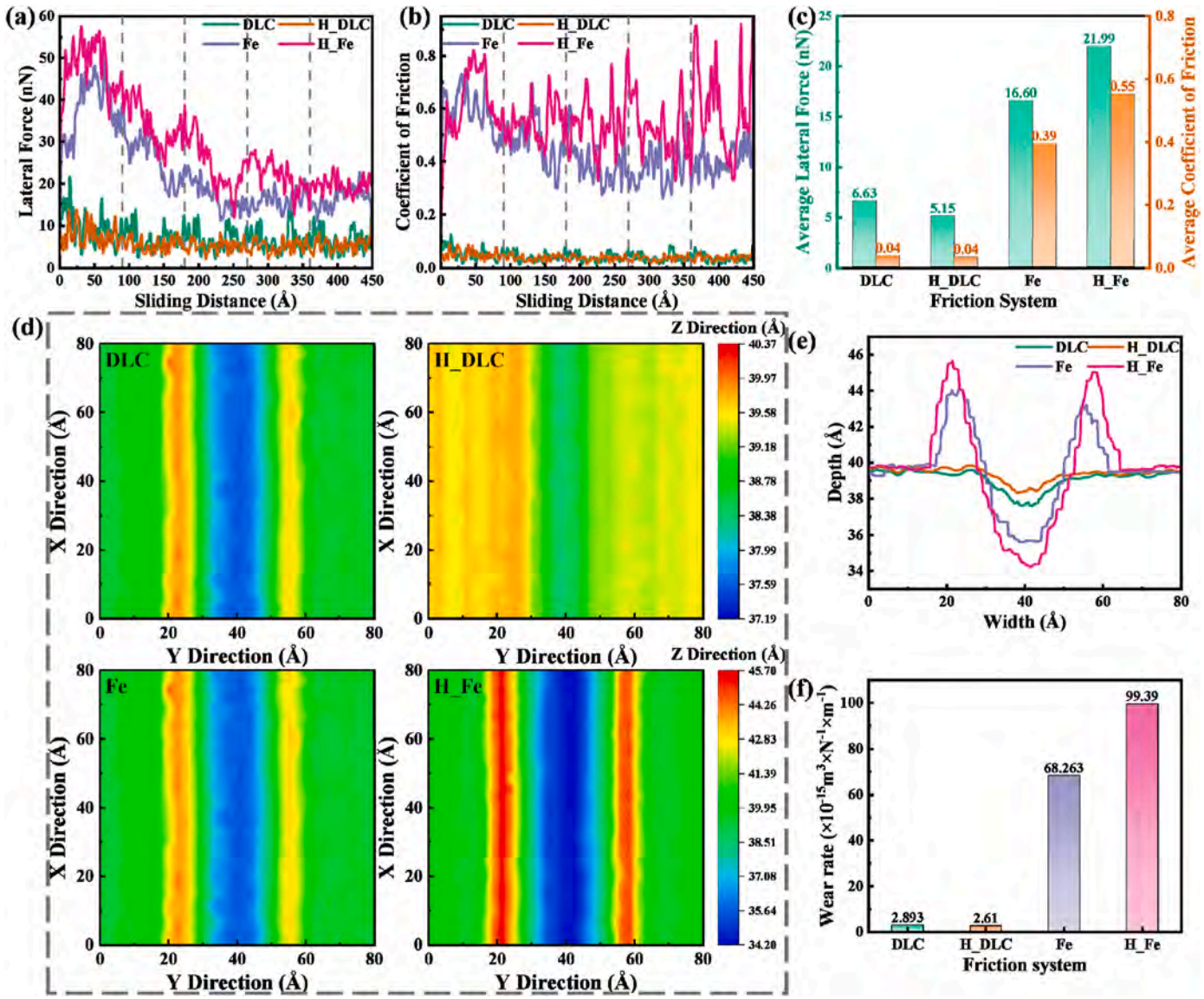

Fig. 4. Comparative analysis of the tribological properties of the non-irradiated and H-atom irradiated systems: (a) Frictional force evolution during sliding cycles; (b) Friction coefficient variation profiles; (c) Quantitative comparison of average frictional force and coefficients; (d) Three-dimensional wear scar topographic maps; (e) Cross-sectional wear scar morphology analysis; (f) Average wear rates.

H-atom irradiation slightly reduces the friction force to 5.15 nN while maintaining the same coefficient. In contrast, the Fe substrate exhibits higher frictions (16.60 nN, 0.39), which increases to 21.99 nN and 0.55 after H-atom irradiation, demonstrating substantial degradation.

The wear scar analysis (Fig. 4d–e) reveals distinct morphological differences. The H_Fe surface shows pronounced wear marks (blue low-value area) and wear debris (red-yellow high-value area). Conversely, the DLC samples retain relatively smooth surfaces [57], with H_DLC showing further wear reduction. The wear rate calculations (Fig. 4f) indicate that H-atom irradiation decreases the DLC wear rates from $2.893 \times 10^{-15}\ m^3 \times N^{-1} \times m^{-1}$ to $2.61 \times 10^{-15}\ m^3 \times N^{-1} \times m^{-1}$, while increasing the Fe substrate wear rates from $6.826 \times 10^{-14}\ m^3 \times N^{-1} \times m^{-1}$ to $9.939 \times 10^{-14}\ m^3 \times N^{-1} \times m^{-1}$. Analysis of the wear scar evolution for different cycles (Fig. S5) demonstrates that primary wear occurs during the first cycle, and subsequent cycles show reduced wear atom counts, consistent with the observed friction evolution. These findings collectively demonstrate that, compared with the deterioration of the tribological properties of the Fe substrate caused by H atom irradiation, the DLC coating not only maintains excellent tribological stability after the same irradiation, but also shows a trend of improved performance in key properties (The data demonstrate a 22.3 % decrease in friction coefficient and a 9.8 % decrease in wear rate of the DLC coating when exposed to H atoms, in comparison to the unirradiated original DLC coating.) compared to the unirradiated original DLC coating.

3.3. *Irradiation-induced microstructural modification of friction surfaces*

The distribution of shear strain on the surface of non-irradiated (Fe) and H-atom irradiation (H_Fe) Fe substrates is illustrated in Fig. 5a1-a5 and 5b1-b5, respectively. The pronounced accumulation of Fe atoms ahead of the friction pair demonstrates that both Fe and H_Fe models experience substantial abrasive wear in the initial friction stage. This phenomenon leads to the concentration of shear stress primarily on the abrasive particles composed of accumulated Fe atoms in front of the friction pair. As the interfacial accumulation of abrasive particles reaches a critical level, the shear strain progressively localizes in the wear debris regions flanking the wear scar.

In the H_Fe model, with prolonged friction duration, Fe atoms migrate along the trailing edge of the frictional counterpart, signifying a

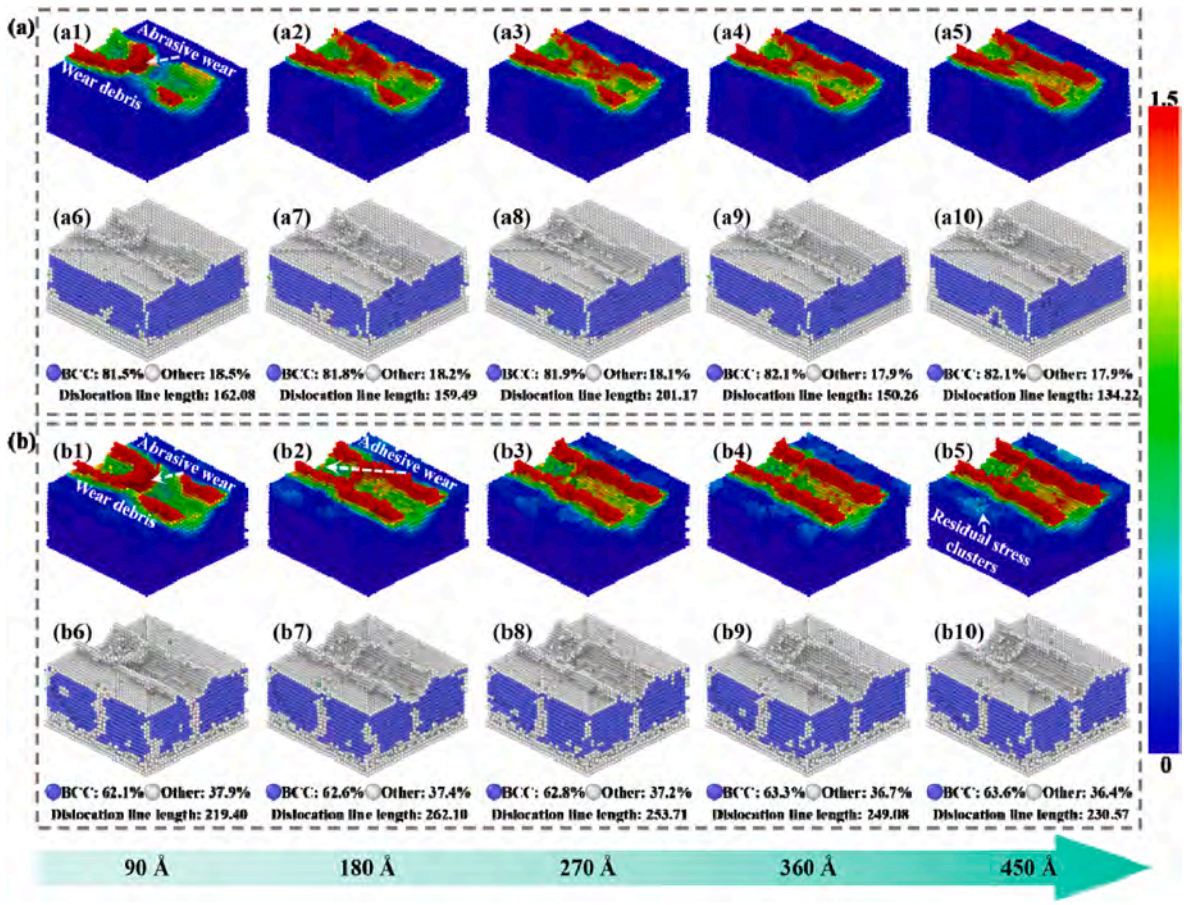

Fig. 5. Surface shear strain and lattice composition analysis of unirradiated (Fe) and H-atom irradiated (H_Fe) Fe substrates: (a1-a5) Interfacial shear strain of unirradiated model with sliding distance, (a6-a10) Change of lattice composition of the unirradiated model with sliding distance, (b1-b5) Change of interfacial shear strain of the H-atom irradiated model with sliding distance, (b6-b10) Change of lattice composition of the H-atom irradiated model with sliding distance.

transition in the wear mechanism from purely abrasive wear to a hybrid mode incorporating both abrasive and adhesive wear components (Fig. S6). This mechanistic transition (Fig. 5b1-b5) results in a higher shear strain distribution at the interface of the H_Fe model and provides direct evidence of the impact of H-atom irradiation on the frictional behavior of the Fe substrate. Notably, the H_Fe model shows conspicuous residual stress clusters on the friction surface (Fig. 5b5), contrasting with the unirradiated Fe model. This phenomenon can be ascribed to lattice defects and localized structural modification due to the diffusion of hydrogen atoms into the substrate. To elucidate the influence of H-atom irradiation on the tribological properties of the Fe substrate, the evolution of lattice structure with sliding distance is analyzed. The H_Fe model shows a more pronounced phase transformation during friction compared to its unirradiated counterpart. Furthermore, the interfacial dislocation line density in the H_Fe model substantially exceeds that of the unirradiated model, corroborating that hydrogen atom diffusion facilitates lattice defect formation and dislocation multiplication [58, 59]. The accumulation of these defects and dislocations profoundly influences the characteristics of interfacial stress distribution and shear behavior at the frictional interface.

In conclusion, H-atom irradiation produces significant microstructural modification in the Fe substrate, including lattice phase transformation and interfacial defect formation. The diffusion behavior of hydrogen atoms promotes lattice phase transition and dislocation proliferation [59], consequently altering the friction properties. These microstructural changes enhance the interfacial stress concentration and strain distribution heterogeneity, ultimately affecting the wear mechanism and interfacial shear stress distribution.

Fig. 6 illustrates the microstructural evolution and interfacial strain distributions of the non-irradiated (DLC) and hydrogen-atom irradiated (H_DLC) DLC coatings. A graphite-like multi-group six-membered ring structure emerges at the wear scar of the DLC model (Fig. 6a1-a3) under frictional shear stress. The progressive transformation of interfacial carbon chains into graphene-like six-membered rings is demonstrated in Fig. 6a7-a9. These structural formations provide substantial evidence for system stabilization during friction and contribute to the stabilization of the friction coefficients. Furthermore, the presence of six-membered ring structures corroborates the theoretical framework suggesting that DLC coatings can develop sp^2 hybrid bonding configurations under mechanical shear stress [60–62]. Notably, the graphitized structure in the wear scar region exhibits instability. The reciprocating shear action of the frictional counterpart system induces continuous bond-breaking and reformation cycles in these six-membered rings (Fig. 6a4-a6). This dynamic process accounts for the pronounced fluctuations observed from the friction and coefficient curves of DLC coatings (Fig. 4a and b). Stress distribution analysis indicates that hydrostatic stress in the interfacial region is predominantly concentrated at the wear scar (Fig. 6a10-a12), while the von Mises stress demonstrates a progressive increase throughout the friction process (Fig. 6a13-a15). This stress evolution (Fig. 6a15) ultimately leads to substantial strain concentration at the wear scar. The structural instability of interfacial six-membered rings during friction tests can be directly correlated with the increase in interfacial stress and its spatial distribution characteristics.

In contrast, the H_DLC coating exhibits a markedly different behavior. The graphitized six-membered rings formed at the interface of H-atom irradiation coatings maintain structural stability throughout the friction process without significant bond rearrangement (Fig. 6b1-b3). The enhanced stability can be primarily attributed to the incorporation

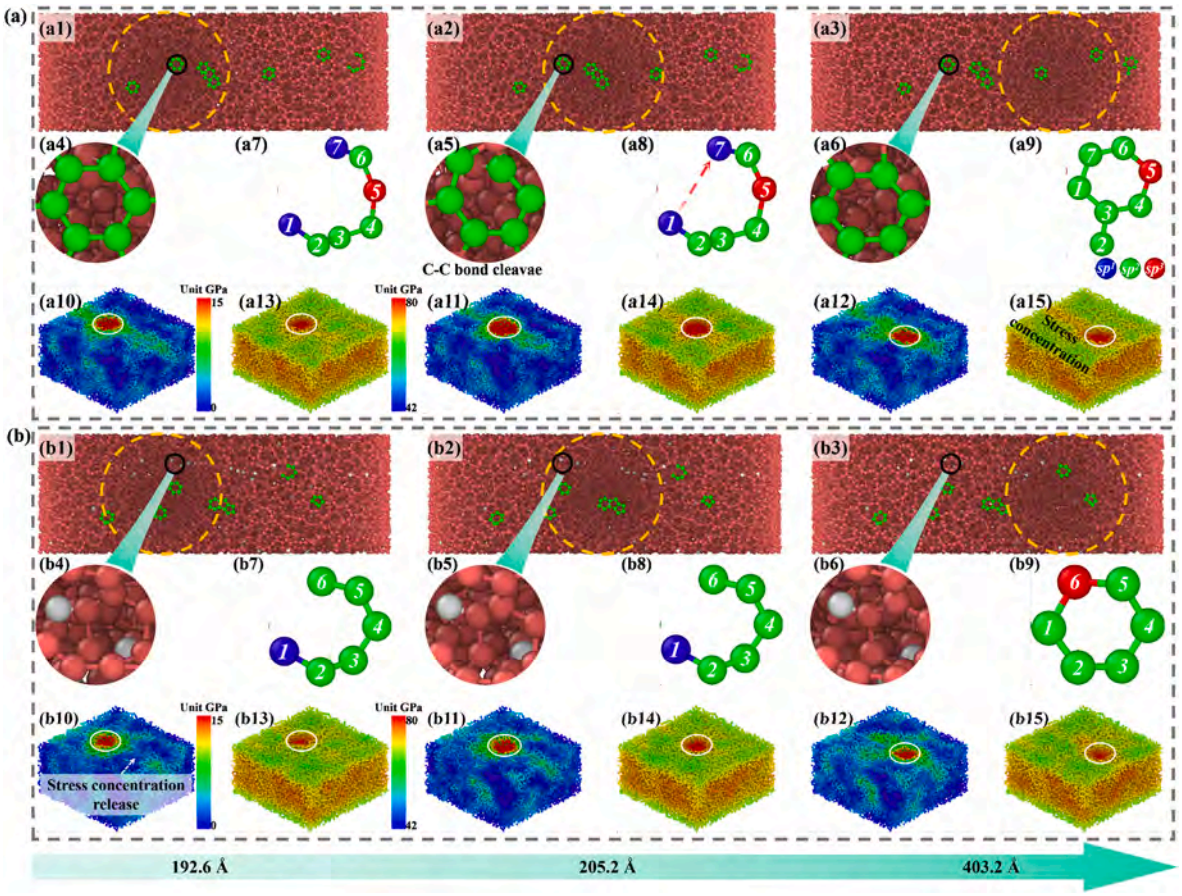

Fig. 6. Analysis of the microstructure and interfacial strain of unirradiated (DLC) and hydrogen-atom irradiated (H_DLC) diamond-like carbon coatings: (a) Unirradiated DLC coatings: Microstructural evolution in the wear scar region (a1-a3), Transformation of graphite-like six-membered ring structures in the wear scar (a4-a6), Detailed progression of graphite-like six-membered ring structure formation (a7-a9), Hydrostatic stress distribution analysis (a10-a12), Von Mises stress evolution with sliding distance (a13-a15); (b) H-atom irradiation DLC (H_DLC) coatings analysis: Microstructural modification (b1-b3), Evolution of graphitized six-membered ring structures (b4-b6), Detailed transformation process of graphitized six-membered ring structures (b7-b9), Hydrostatic stress distribution changes (b10-b12), Von Mises stress variation with sliding distance (b13-b15).

of hydrogen atoms. The stabilization mechanism operates through two distinct pathways: (1) Hydrogen atoms form robust covalent bonds with dangling carbon bonds (Fig. S7) and maintain the C–H bond integrity during friction (Fig. 6b4-b7) and (2) H-atom irradiation substantially reduces interfacial stress. This reduction is evidenced by the lower hydrostatic stress (Fig. 6b10-b12) and von Mises stress (Fig. 6b13-b15) compared to the unirradiated DLC model, accompanied by effective strain release. As shown in the stacked bar diagram of interface stress distribution in Fig. S8, the H_DLC model exhibits the following changes in hydrostatic stress: the proportion of the 10–15 GPa interval decreases; the proportion of the 5–10 GPa interval increases; and the proportion of the <5 GPa interval also declines. Regarding von Mises stress, the H_DLC model shows that the proportion in the 70–80 GPa interval decreases, while the proportions in the 60–70 GPa and <60 GPa intervals increase. In summary, the DLC's response to irradiation results in a shift towards lower stress levels. Comparative analysis of interfacial shear strain further confirms that the H_DLC coatings exhibit lower shear strain than the unirradiated coatings (Fig. S9). These findings demonstrate that H-atom irradiation mitigates the fracture and recombination of graphitized six-membered ring structures during friction tests by optimizing the interfacial stress distribution characteristics and reducing the shear strain. Consequently, this process enhances the durability and stability.

Fig. 7a and b present the evolution of hybrid bonding configurations in both unirradiated (DLC) and H-atom irradiated (H-DLC) DLC coatings during friction tests. When the sliding distance is 0 Å, that is, before the friction starts, the sp^3 bond content of the DLC film irradiated by H atoms (9.9 %) is higher than that of the unirradiated DLC coating (9.6 %). The data reveal a progressive reduction in sp^1 hybridized bonds in both DLC and H-DLC systems as friction progresses due to the stress-induced reconfiguration of surface carbon atoms under compressive loading [63]. Compared to the H-DLC system, the DLC interface maintains a higher concentration of sp^2 bonds.

To elucidate the mechanistic influence of H-atom irradiation on the structural evolution of DLC coatings during tribological processes, the hybrid bond transformations in the wear scar interface are studied (x: 0–90 Å, y: 25–55 Å, z: 39–45 Å, as detailed in Fig. S10). Fig. 7c and d reveal larger fluctuations in the sp^2 and sp^3 contents at the DLC friction interface compared to the H-DLC coating, suggesting that irradiation with hydrogen atoms increases the structural stability of the DLC coating, in agreement with Fig. 3g. This improvement primarily arises from that the hydrogen-mediated modulation of carbon bonding states increases the sp^3 hybrid bonds at the friction interface., thus enhancing the compressive strength and suppressing fracture of interfacial carbon bonds [61,64,65]. The hydrogen permeation-induced structural stabilization mechanism of the DLC coating enhances both the wear resistance and long-term operational stability of the system.

Fig. 8a and b present the atomic configurations of carbon atoms in the DLC coatings at the friction termination stage analyzed by the Voronoi tessellation methodology [23,66]. Both the unirradiated (DLC) and H-atom irradiated (H-DLC) coatings show 17–19 face polyhedra. H-atom irradiation increases the population of 15-face and 17-face polyhedra, demonstrating the influence of hydrogen atoms on the

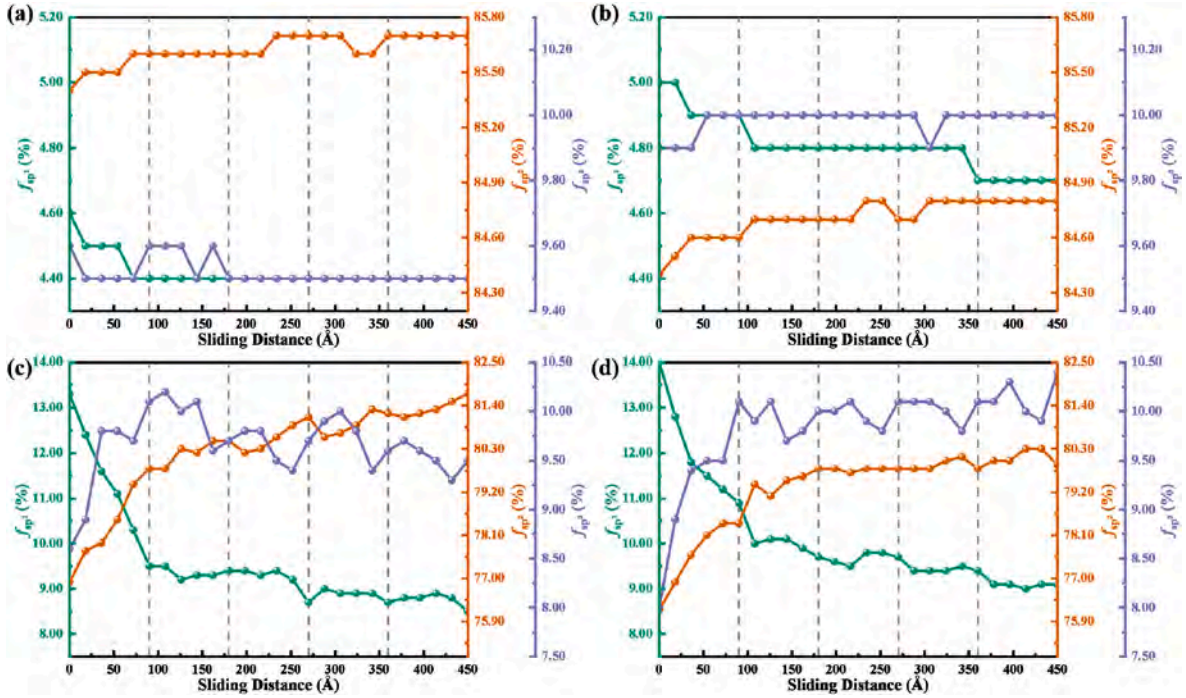

Fig. 7. Analysis of the hybrid bond contents in non-irradiated (DLC) and H-atom irradiated (H_DLC) DLC coatings (**The green, orange, and purple lines represent changes in sp^1, sp^2, and sp^3 bond content, respectively**): (a) Change of the hybrid bond content in non-irradiated DLC coatings, (b) Change of the hybrid bond content in H-atom irradiated DLC coatings, (c) Change of the hybrid bond content at the wear marks of non-irradiated DLC coatings, (d) Change of the hybrid bond content at the wear marks of H-atom-irradiated DLC coatings. (For interpretation of the references to color in this figure legend, the reader is referred to the Web version of this article.)

atomic stacking configurations. Gaussian distribution analysis reveals reduced peak intensity after H-atom irradiation. Both systems display distinct three-fold and four-fold symmetries (Fig. 8b), and the Gaussian fitting curves of the Voronoi polyhedron edge numbers mirror the facet distribution trends.

The spatial non-uniformity of the atomic distributions is quantitatively characterized using the local spatial non-uniformity parameter (h), as shown in Fig. 8c. H-atom irradiation reduces the initial h value from 0.34 to 0.31, indicating enhanced structural ordering. Comparing the data at the end of the friction process, the structural ordering of both coatings shows significant improvement, with the unirradiated DLC exhibiting an increase of 14.7 % and the H-DLC system 19.4 %. The differential enhancement confirms hydrogen's efficacy in promoting the transition of plastic deformation regions from disordered to ordered states, consistent with the observed sp^3 hybridization trends at the interface (Fig. 7). Frictional interface temperature monitoring (Fig. 8d) reveals lower thermal generation in the H-DLC coatings, further corroborating the enhanced stability by hydrogen incorporation. The temperature variation clouding diagram of the friction interface is shown in Fig. S11. The interface temperature of both systems is below the hybrid bond transition threshold (1000 K), indicating that interfacial bond transformations are predominantly stress-mediated rather than thermally activated [67]. In conclusion, hydrogen incorporation optimizes the structure *via* enhanced atomic ordering and improved interfacial strain distributions. Structural modification improves the stability of graphitic six-membered rings and mitigates interfacial fracturing and reorganization through localized stress reduction.

3.4. Experimental validation

To validate the simulation results, DLC coatings are fabricated by DC magnetron sputtering and then undergo H-atom irradiation. The results reveal a thinner coating after H-atom irradiation due to etching (Fig. S12) [24,68,69]. The surface morphology changes after hydrogen bombardment, showing diminishing or disappearing cauliflower-like structures and improved planarity and uniformity (Fig. S12–S14). To ensure the experimental reliability, tribological testing was performed on both diamond-like carbon (DLC) coatings and iron substrates subjected to pure Ar plasma treatment (Fig. S15). The experimental results revealed that pure Ar plasma treatment reduces the initial friction coefficient of the Fe substrate (Fig. S15a), which can be attributed to the surface cleaning effect induced by Ar plasma. Subsequently, the friction coefficient demonstrated a gradual increase, though with smaller amplitude fluctuations compared to Fe substrates treated with Ar/H_2 mixed plasma. This contrast further confirms the critical role of hydrogen components in chemically modulating the friction interface. For DLC coatings, the friction coefficient of Ar-treated specimens began decreasing at approximately 1100 s, while those treated with Ar/H_2 plasma entered the friction reduction and stabilization phase around 700 s (Fig. S15a). Raman spectroscopy analysis revealed distinct structural changes: the I_D/I_G ratio showed a slight decrease from 1.07 to 1.01 for pure Ar treatment, compared to a more substantial reduction to 0.95 for Ar/H_2 treatment (Fig. S15b and Fig. 9e). These results indicate that hydrogen more effectively facilitates the reconstruction of carbon bond structures at the DLC interface. In summary, it is reliable to use a mixture of Ar/H_2 mixed plasma instead of pure H_2 plasma in this study. Tribological evaluation is conducted by systematic friction tests on the uncoated substrates and DLC coatings, as shown in Fig. 9a–c. The H-atom irradiated DLC coatings have reduced friction coefficients and enhanced wear resistance, while the uncoated substrate shows a contrasting behavior. The experimental results indicate that the friction coefficient (CoF) of the iron matrix increased from 0.46 to 0.61 after irradiation, representing a 32.61 % rise. The wear rate rose from $620.58 \times 10 \times 10^{-7}\ m^3 \times N^{-1} \times m^{-1}$ to $744.08 \times 10^{-7}\ m^3 \times N^{-1} \times m^{-1}$, a 19.90 % increase. For the DLC coating, the friction coefficient decreased from 0.30 to 0.26 (a 13.33 % reduction), while the wear rate dropped from $7.31 \times 10^{-7}\ m^3 \times N^{-1} \times m^{-1}$ to $3.16 \times 10^{-7}\ m^3 \times N^{-1} \times m^{-1}$, marking a 56.77 % reduction. The simulation results show that after irradiation,

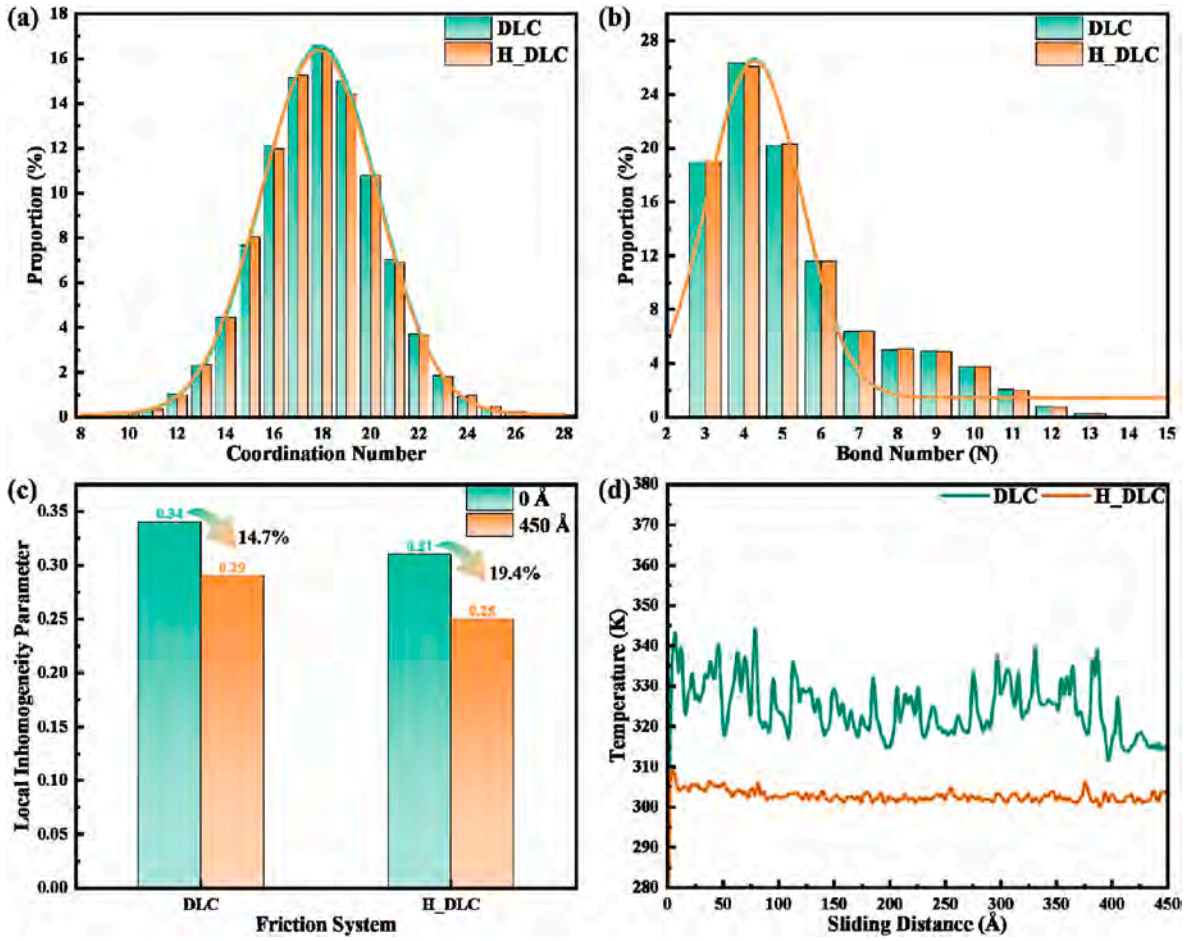

Fig. 8. Changes in the parameters of unirradiated (DLC) and H-atom irradiated (H_DLC) DLC coatings during friction tests: (a) Changes in the number of Voronoi polyhedron faces with the curve in the graph being the Gaussian fit corresponding to the color of the bar graph; (b) Changes in the number of Voronoi polyhedron edges with the curve in the graph being the Gaussian fit corresponding to the color of the bar graph; (c) Changes in the local spatial non-uniformity; (d) Changes in the interface temperature during friction. (For interpretation of the references to color in this figure legend, the reader is referred to the Web version of this article.)

the friction coefficient of the iron matrix increased from 0.39 to 0.55 (a 41.03 % increase). The wear rate rose from 68.263 × 10^{-15} m^3 × N^{-1} × m^{-1} to 99.39 × 10^{-15} m^3 × N^{-1} × m^{-1}, a 45.60 % rise. The friction coefficient of the DLC coating remained stable at 0.04. Its wear rate decreased from 2.893 × 10^{-15} m^3 × N^{-1} × m^{-1} to 2.61 × 10^{-15} m^3 × N^{-1} × m^{-1}, a 9.78 % drop. The trends in the experimentally measured friction coefficients and wear rates (Fig. 9a–c and Fig. S14) align well with the simulation results (Fig. 4), considering the significant scale differences and inherent simplifications of the simulation model. Microstructural characterization is performed by Raman scattering, and Gaussian deconvolution shows peaks at 1380 cm^{-1} (D band representing disordered structures) and 1560 cm^{-1} (G band corresponding to graphitic structures) from both the unirradiated and H-atom irradiated coatings (Fig. 9d and e). Fig. 9d and e show that the I_D/I_G ratio of the unirradiated sample exhibits a minimal increase of approximately 0.01 following friction. This change aligns with the molecular dynamics simulation results (Fig. 7). These findings suggest that transiently formed graphene-like structures lack thermodynamic stability. In contrast, the irradiated sample shows a more pronounced I_D/I_G ratio increase of ~0.08 post-friction, indicative of enhanced sp^2 bond formation at the interface. This observed trend corresponds well with simulation predictions (Fig. 7), where hydrogen irradiation facilitates structural modifications that promote sp^2 hybridization during tribological processes. [70,71], consistent with Figs. 6 and 7. X-ray photoelectron spectroscopy (XPS) confirms the larger sp^3 content after H-atom irradiation in agreement with Fig. 7. The observed decrease in the I_D/I_G ratio after H-atom irradiation (Fig. 9d and e) stems from the passivation of dangling carbon bonds by hydrogen atoms, which promotes the formation of sp^3 hybridized bonds and enhances interfacial structural ordering. The experimental findings are in excellent agreement with the simulation results in Fig. 8.

4. Discussion

According to the simulated and experimental results, a friction model is established to elucidate the influence of H-atom irradiation on the tribological behavior and underlying mechanisms of the Fe substrate and DLC coating, as shown in Fig. 10. The diffusion dynamics of irradiated hydrogen atoms in the Fe substrate modifies the microstructure by primarily generating surface defects and proliferating dislocations (Fig. 10b) [47–49,58]. These microstructural alterations change the transition in the friction mechanism of the Fe substrate from conventional abrasive wear to a composite wear mode incorporating both abrasive and adhesive components (Fig. 10d). In this composite mode, the interfacial stress and strain concentrations are amplified due to enhanced adhesion between abrasive particles and the Fe substrate, ultimately compromising the friction through intensified localized wear. With regard to the DLC coatings, H-atom irradiation shows a distinct mechanism. As shown in Fig. 10c, the primary interactions between irradiating hydrogen atoms and the DLC coating occur through C–H bond formation and pore binding [54,55]. These interactions yield two significant benefits: (1) enhancement of the coating structure and

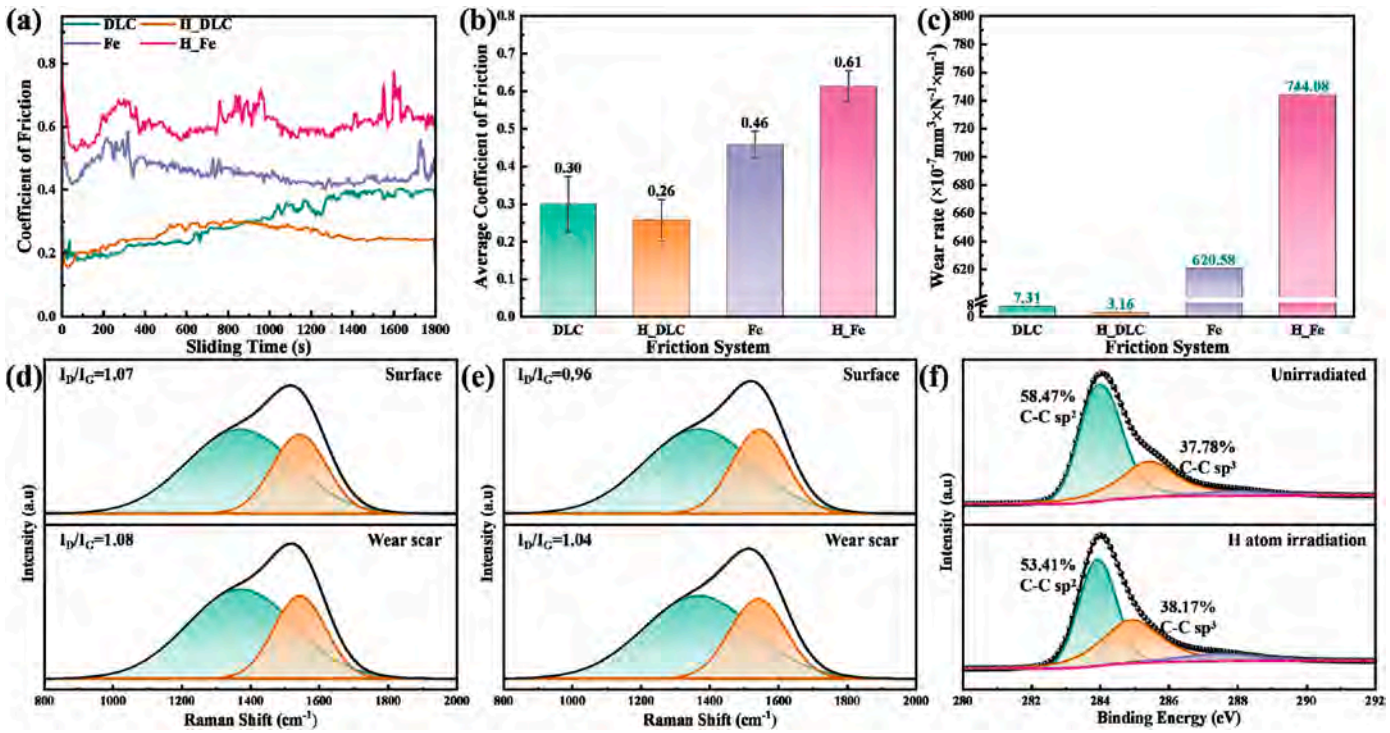

Fig. 9. Experimental results of unirradiated and H-atom irradiated samples: (a) Friction coefficient curves, (b) Average friction coefficients, (c) Wear volumes, (d) Raman spectra of unirradiated DLC coating surface and wear pit, (e) Raman spectra of H-atom irradiated DLC coating surface and wear pit, (f) XPS spectra of unirradiated and H-atom irradiated DLC coating.

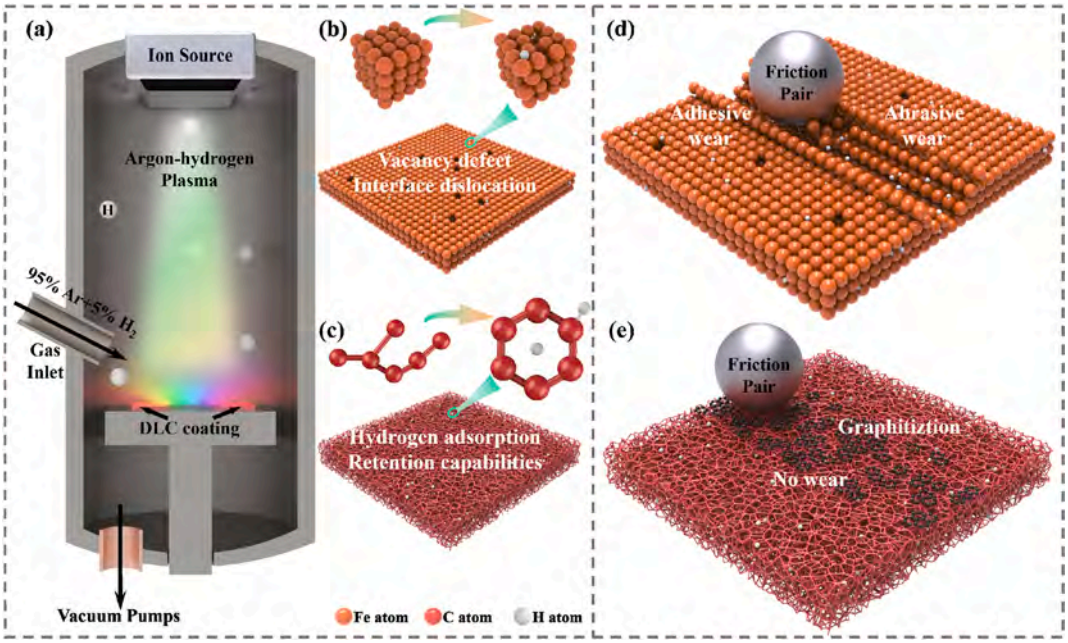

Fig. 10. Mechanism of the friction properties of amorphous carbon films after H-atom irradiation: (a) Schematic diagram of the experimental process of H-atom irradiation, (b) Effects of H-atom irradiation on the Fe substrate structure, (c) Effects of H-atom irradiation on the DLC layer structure, (d) Friction mechanism of H-atom irradiation on the Fe substrate, (e) Friction mechanism of H-atom irradiation on the DLC layer.

ordering, and (2) reduction of the interfacial interaction energy [36,72,73], which facilitates strain relaxation at the interface. The graphitized six-membered ring structures, initially susceptible to stress concentration, have improved stability during friction due to hydrogen atom interactions. This stabilization effect enables gradual interfacial strain release to prevent structural fracture or slip. Consequently, the coating has substantially better wear resistance and durability in the friction test.

5. Conclusions

Molecular dynamics simulations and experimental investigations are

performed to systematically analyze the diffusion behavior of hydrogen atom irradiation on the material properties and the impact on the interfacial structural evolution between the Fe substrate and DLC coating. Our findings reveal that the DLC coating shows approximately three orders of magnitude better hydrogen permeation barrier properties than the Fe substrate. H-atom irradiation enhances the structural ordering of the film by facilitating the evolution of carbon atom bonding states, as evidenced by Raman scattering and X-ray photoelectron spectroscopy. Tribological evaluations indicate that hydrogen atoms degrade the frictional properties *via* two primary mechanisms: lattice phase transitions in the Fe substrate and generation of interfacial defects. Conversely, H-atom irradiation enhances the durability of the six-membered ring structure formed at the friction interface by optimizing the strain distributions at the DLC coating interface and mitigating local stress concentrations. This investigation provides comprehensive atomic-level insights into the structural evolution and tribological properties of DLC coatings upon H-atom irradiation and valuable guidance for their implementation in semiconductor applications.

CRediT authorship contribution statement

Hu Zhang: Writing – original draft, Visualization, Validation, Software, Methodology, Investigation, Formal analysis, Data curation, Conceptualization. **Shu Xiao:** Writing – review & editing, Validation, Supervision, Resources, Project administration, Investigation, Funding acquisition, Data curation, Conceptualization. **Yong Huang:** Visualization, Investigation, Data curation. **Qingdong Ruan:** Methodology, Formal analysis, Conceptualization. **Guohua Chen:** Validation, Methodology, Investigation, Conceptualization. **Saihua Jiang:** Visualization, Methodology, Conceptualization. **Chao Yang:** Visualization, Validation, Supervision, Software, Methodology, Formal analysis, Conceptualization. **Paul K. Chu:** Writing – review & editing, Formal analysis, Conceptualization.

Declaration of competing interest

The authors declare that they have no known competing financial interests or personal relationships that could have appeared to influence the work reported in this paper.

Acknowledgments

This work is supported by the National Natural Science Foundation of China (No. 52375182), Natural Science Foundation of Guangdong Province (No. 2023A1515012308), Basic and Applied Basic Research Foundation of Guangzhou (No.2024A04J3821), Guangdong Province Science and Technology Plan Projects (No.s 2023B1212060045 and 2023B1212120008), Basic and Applied Basic Research Fund of Guangdong Province (No. 2024A1515010452), as well as City University of Hong Kong Donation Research Grants (No. DON-RMG 9229021 and No. 9229021).

Appendix A. Supplementary data

Supplementary data to this article can be found online at https://doi.org/10.1016/j.carbon.2025.120658.

References

[1] H.C. Barshilia, A. Ananth, J. Khan, G. Srinivas, Ar+H_2 plasma etching for improved adhesion of PVD coatings on steel substrates, Vacuum 86 (8) (2012) 1165–1173.
[2] P. Cotterill, P. Cotterill, The hydrogen embrittlement of metals, Prog. Mater. Sci. 9 (4) (1961) 205–301.
[3] B. Zhang, Q. Zhu, C. Xu, C. Li, Y. Ma, Z. Ma, S. Liu, R. Shao, Y. Xu, B. Jiang, L. Gao, X. Pang, Y. He, G. Chen, L. Qiao, Atomic-scale insights on hydrogen trapping and exclusion at incoherent interfaces of nanoprecipitates in martensitic steels, Nat. Commun. 13 (1) (2022) 3858.
[4] Q. Liu, Q. Zhou, J. Venezuela, M. Zhang, A. Atrens, Hydrogen influence on some advanced high-strength steels, Corros. Sci. 125 (2017) 114–138.
[5] X.-F. Zhang, Z.-W. Kan, Y. Yang, Y.-X. Wan, J.-X. Li, Z.-Y. Huang, Investigation of the effect of electrolytic hydrogen charging on tensile-ductility loss in different Al-added low density steels, Mater. Sci. Eng., A 795 (2020) 140027.
[6] M.A. Mohtadi-Bonab, M. Masoumi, Different aspects of hydrogen diffusion behavior in pipeline steel, J. Mater. Res. Technol. 24 (2023) 4762–4783.
[7] Q. He, T.-Y. Sun, L.-F. Huang, Chemical-bonding and lattice-deformation mechanisms unifying the stability and diffusion trends of hydrogen in TiN and AlN polymorphs, Acta Mater. 281 (2024) 120447.
[8] L. Luo, M. Su, P. Yan, L. Zou, D.K. Schreiber, D.R. Baer, Z. Zhu, G. Zhou, Y. Wang, S.M. Bruemmer, Z. Xu, C. Wang, Atomic origins of water-vapour-promoted alloy oxidation, Nat. Mater. 17 (6) (2018) 514–518.
[9] X.Y. Cheng, H.X. Zhang, A new perspective on hydrogen diffusion and hydrogen embrittlement in low-alloy high strength steel, Corros. Sci. 174 (2020) 108800.
[10] M.R. Price, B. Raeymaekers, Quantifying adhesion of ultra-thin multi-layer DLC coatings to Ni and Si substrates using shear, tension, and nanoscratch molecular dynamics simulations, Acta Mater. 141 (2017) 317–326.
[11] C. Androulidakis, E.N. Koukaras, G. Paterakis, G. Trakakis, C. Galiotis, Tunable macroscale structural superlubricity in two-layer graphene via strain engineering, Nat. Commun. 11 (1) (2020) 1595.
[12] W. Zhai, K. Zhou, Nanomaterials in superlubricity, Adv. Funct. Mater. 29 (28) (2019) 1806395.
[13] N. Boutroy, Y. Pernel, J.M. Rius, F. Auger, H.J.v. Bardeleben, J.L. Cantin, F. Abel, A. Zeinert, C. Casiraghi, A.C. Ferrari, J. Robertson, Hydrogenated amorphous carbon film coating of PET bottles for gas diffusion barriers, Diam. Relat. Mater. 15 (4–8) (2006) 921–927.
[14] D.-H. Shin, S.-J. Kim, Effect of hydrogen embrittlement on mechanical characteristics of DLC-coating for hydrogen valves of FCEVs, npj Mater. Degrad. 8 (1) (2024) 47.
[15] G.D. Tolstolutska, M.O. Azarenkov, V.A. Bilous, O.S. Kuprin, M.G. Ishchenko, Hydrogen Barrier Coatings and their Permeation Resistance, Problems of Atomic Science and Technology 2024, 2024, pp. 100–117.
[16] G.A. Abbas, S.S. Roy, P. Papakonstantinou, J.A. McLaughlin, Structural investigation and gas barrier performance of diamond-like carbon based films on polymer substrates, Carbon 43 (2) (2005) 303–309.
[17] WX. Wu, H.X. Liu, X.M. Jin, L.L. Guo, T. Zhu, L.B. Hu, C. Yang, P.H. Chen, C.J. Qiu, P.K. Chu, Unveiling high-temperature tribological behavior and wear mechanism of WCp/HEA composite coating via laser additive manufacturing, Ceram. Int. 51 (2025) 19485–19496.
[18] C. Yang, T. Ying, A.H. Huang, J. Huang, P.H. Chen, P.K. Chu, X.Q. Zeng, Enhancing the corrosion resistance of MAO coatings on LY12 alloy by in situ co-doping with zinc phosphate and cerium phosphate, Corros. Commun 17 (2025) 35–43.
[19] B. Sun, W. Lu, B. Gault, R. Ding, S.K. Makineni, D. Wan, C.-H. Wu, H. Chen, D. Ponge, D. Raabe, Chemical heterogeneity enhances hydrogen resistance in high-strength steels, Nat. Mater. 20 (12) (2021) 1629–1634.
[20] M. Tamura, T. Kumagai, Hydrogen permeability of diamondlike amorphous carbons, J. Vac. Sci. Technol. A: Vacuum, Surfaces, and Films 35 (4) (2017).
[21] V.R. Salinas Ruiz, T. Kuwahara, J. Galipaud, K. Masenelli-Varlot, M.B. Hassine, C. Héau, M. Stoll, L. Mayrhofer, G. Moras, J.M. Martin, M. Moseler, M.-I. de Barros Bouchet, Interplay of mechanics and chemistry governs wear of diamond-like carbon coatings interacting with ZDDP-additivated lubricants, Nat. Commun. 12 (1) (2021) 4550.
[22] M. Moseler, P. Gumbsch, C. Casiraghi, A.C. Ferrari, J. Robertson, The ultrasmoothness of diamond-like carbon surfaces, Science 309 (5740) (2005) 1545–1548.
[23] Y. Shi, Q. Xia, M. Xie, Q. Zhou, D. Hua, L. Chai, T. Shi, S.J. Eder, H. Wang, P. Wang, W. Liu, Insights into irradiation-affected structural evolution and mechanical behavior of amorphous carbon, Acta Mater. 281 (2024) 120424.
[24] P. Shi, L. Chen, J. Xu, L. Qian, M. Kubo, Y. Wang, Unveiling the interaction regimes between atomic oxygen and amorphous carbon surface depending on incident energy, Carbon 226 (2024) 119229.
[25] F. Valencia, J.D. Mella, R.I. González, M. Kiwi, E.M. Bringa, Confinement effects in irradiation of nanocrystalline diamond, Carbon 93 (2015) 458–464.
[26] S. Yang, L. Zhang, Advancing damage-free machining of KDP: a comprehensive review, J. Am. Ceram. Soc. 108 (4) (2025) 20341.
[27] S. Plimpton, S. Plimpton, Fast parallel algorithms for short-range molecular dynamics, J. Comput. Phys. 117 (1) (1995) 1–19.
[28] A. Stukowski, Structure identification methods for atomistic simulations of crystalline materials, Model. Simulat. Mater. Sci. Eng. 20 (4) (2012) 045021.
[29] S.J. Stuart, A.B. Tutein, J.A. Harrison, A reactive potential for hydrocarbons with intermolecular interactions, J. Chem. Phys. 112 (14) (2000) 6472–6486.
[30] J. Tersoff, New empirical model for the structural properties of silicon, Phys. Rev. Lett. 56 (6) (1986) 632–635.
[31] M. Wen, A new interatomic potential describing Fe-H and H-H interactions in bcc iron, Comput. Mater. Sci. 197 (2021) 110640.
[32] X. Yang, R. Li, Y. Wang, J. Zhang, Tunable, Wide-Temperature, and Macroscale Superlubricity Enabled by Nanoscale Van Der Waals Heterojunction-to-Homojunction Transformation, Adv. Mater. 35 (39) (2023) 2303580.
[33] Z. Lan, Y.Q. Sun, L.Q. Wang, L. Ming, Molecular dynamics simulation of diamond cutting iron with water lubrication, J. Phys. Conf. 1748 (6) (2021) 062048.
[34] Y. Liu, J. Xie, L. Tang, Design and evaluation method of erosion-resistant and wear-resistant CoCrFeMnNi high-entropy alloy coating based on molecular dynamics simulation and machine learning, Corros. Sci. 254 (2025) 113048.

[35] S. Yang, L. Zhang, Z. Wu, Effect of anisotropy of potassium dihydrogen phosphate crystals on its deformation mechanisms subjected to nanoindentation, ACS Appl. Mater. Interfaces 13 (34) (2021) 41351–41360.
[36] Y. Wang, J. Xu, Y. Ootani, S. Bai, Y. Higuchi, N. Ozawa, K. Adachi, J.M. Martin, M. Kubo, Tight-binding quantum chemical molecular dynamics study on the friction and wear processes of diamond-like carbon coatings: effect of tensile stress, ACS Appl. Mater. Interfaces 9 (39) (2017) 34396–34404.
[37] P. Li, W. He, P. Ju, L. Ji, X. Liu, F. Wu, Z. Lu, H. Li, L. Chen, J. Liu, H. Zhou, J. Chen, Acquisition of molecular rolling lubrication by self-curling of graphite nanosheet at cryogenic temperature, Nat. Commun. 15 (1) (2024) 5747.
[38] H. Hu, J. Wang, K. Tian, Q. Zheng, M. Ma, The effects of disordered edge and vanishing friction in microscale structural superlubric graphite contact, Nat. Commun. 15 (1) (2024) 10830.
[39] X. Li, A. Wang, K.-R. Lee, Comparison of empirical potentials for calculating structural properties of amorphous carbon films by molecular dynamics simulation, Comput. Mater. Sci. 151 (2018) 246–254.
[40] X.H. Long, W. Setyawan, K.P. Tai, Y. Liu, M.S. Yu, Z.Q. Wang, N. Gao, X.L. Wang, Defect formation and bending properties in graphite under He atom implantation investigated by molecular dynamics method, Carbon 191 (2022) 350–361.
[41] X. Li, X. Xu, Y. Zhou, K.-R. Lee, A. Wang, Insights into friction dependence of carbon nanoparticles as oil-based lubricant additive at amorphous carbon interface, Carbon 150 (2019) 465–474.
[42] H.-K. Kim, M. Lee, K.-R. Lee, J.-C. Lee, How can a minor element added to a binary amorphous alloy simultaneously improve the plasticity and glass-forming ability? Acta Mater. 61 (17) (2013) 6597–6608.
[43] S.Z. Chavoshi, X. Luo, Molecular dynamics simulation study of deformation mechanisms in 3C-SiC during nanometric cutting at elevated temperatures, Mater. Sci. Eng., A 654 (2016) 400–417.
[44] M.B. Cai, X.P. Li, M. Rahman, Study of the temperature and stress in nanoscale ductile mode cutting of silicon using molecular dynamics simulation, J. Mater. Process. Technol. 192–193 (2007) 607–612.
[45] S. Yang, L. Zhang, Z. Wu, An investigation on the nano-abrasion wear mechanisms of KDP crystals, Wear 476 (2021) 203692.
[46] S. Yang, L. Zhang, Z. Wu, Subsurface damage minimization of KDP crystals, Appl. Surf. Sci. 604 (2022) 154592.
[47] D.E. Jiang, E.A. Carter, Diffusion of interstitial hydrogen into and through bcc Fe from first principles, Phys. Rev. B 70 (6) (2004) 064102.
[48] B. Sun, W. Krieger, M. Rohwerder, D. Ponge, D. Raabe, Dependence of hydrogen embrittlement mechanisms on microstructure-driven hydrogen distribution in medium Mn steels, Acta Mater. 183 (2020) 313–328.
[49] S.P. Lynch, Interpreting hydrogen-induced fracture surfaces in terms of deformation processes: a new approach, Scr. Mater. 65 (10) (2011) 851–854.
[50] X. Xing, F. Li, J. Liu, G. Cui, Z. Li, Y.F. Cheng, Molecular dynamics modeling of hydrogen-induced plastic deformation and cracking of α-iron, J. Mater. Sci. Technol. 176 (2024) 119–131.
[51] J. Song, W.A. Curtin, A nanoscale mechanism of hydrogen embrittlement in metals, Acta Mater. 59 (4) (2011) 1557–1569.
[52] X. Xing, Y. Zhang, S. Wang, Z. Li, C. Yang, G. Cui, S. Zhang, J. Liu, J. Gou, H. Yu, Atomistic simulation of hydrogen-induced plastic zone compression during cyclic loading, Int. J. Hydrogen Energy 45 (31) (2020) 15697–15709.
[53] M.F. Kapci, J.C. Schön, B. Bal, The role of hydrogen in the edge dislocation mobility and grain boundary-dislocation interaction inα-Fe, Int. J. Hydrogen Energy 46 (64) (2021) 32695–32709.
[54] D. Shi, C. Bai, Y. Liu, X. Wang, X. Zhang, J. Zhang, Selective plasma treatment endowing low-friction and wear-resistant surface of polycrystalline diamond against copper, ACS Appl. Mater. Interfaces 16 (43) (2024) 59576–59585.
[55] N. Du, X. Wei, X. Li, Z. Chen, S. Lu, J. Ding, C. Feng, K. Chen, J. Qiao, D. Zhang, K.-R. Lee, Unraveling the friction response from selective hydrogenation of textured amorphous carbon surface, Appl. Surf. Sci. 614 (2023) 156246.
[56] T. Michler, J. Naumann, Coatings to reduce hydrogen environment embrittlement of 304 austenitic stainless steel, Surf. Coating. Technol. 203 (13) (2009) 1819–1828.
[57] Z. Chen, J. Wu, B. Su, Y. Wang, Temperature-structure-induced metastable structural transformation mechanism of the amorphous carbon film during friction, Tribol. Int. 191 (2024) 109112.
[58] S.P. Lynch, Environmentally assisted cracking: overview of evidence for an adsorption-induced localised-slip process, Acta Metall. 36 (10) (1988) 2639–2661.
[59] X. Xing, M. Yu, W. Chen, H. Zhang, Atomistic simulation of hydrogen-assisted ductile-to-brittle transition in α-iron, Comput. Mater. Sci. 127 (2017) 211–221.
[60] R. Brittain, T. Liskiewicz, A. Morina, A. Neville, L. Yang, Diamond-like carbon graphene nanoplatelet nanocomposites for lubricated environments, Carbon 205 (2023) 485–498.
[61] Y. Zhou, Z. Chen, T. Zhang, S. Zhang, X. Xing, Q. Yang, D. Li, Metastable hybridized structure transformation in amorphous carbon films during friction-A study combining experiments and MD simulation, Friction 11 (9) (2023) 1708–1723.
[62] Z. Yue, X. Fan, Y. Wang, H. Li, J. Zhang, M. Zhu, Fretting behaviors of self-mated diamond-like carbon films: the evolution of fretting regime and transfer film, Carbon 203 (2023) 695–705.
[63] X. Li, A. Wang, K.-R. Lee, Insights on low-friction mechanism of amorphous carbon films from reactive molecular dynamics study, Tribol. Int. 131 (2019) 567–578.
[64] L. Li, M. Xu, W. Song, A. Ovcharenko, G. Zhang, D. Jia, The effect of empirical potential functions on modeling of amorphous carbon using molecular dynamics method, Appl. Surf. Sci. 286 (2013) 287–297.
[65] J. Robertson, Diamond-like amorphous carbon, Mater. Sci. Eng. R Rep. 37 (2) (2002) 129–281.
[66] S. Lahkar, R. Ranganathan, Competing mechanisms govern the thermal rectification behavior in semi-stochastic polycrystalline graphene with graded grain-size distribution, Carbon 218 (2024) 118638.
[67] R. Mao, X. Cui, J. Hao, S. Zhao, S. Hou, F. Lan, Y. Li, L. Deng, H. Li, Densification and surface carbon transformation of diamond powders under high pressure and high temperature, Materials 17 (3) (2024) 603.
[68] O.V. Penkov, M. Kheradmandfard, M. Khadem, M. Kharaziha, R. Mirzaamiri, K.-J. Seo, D.-E. Kim, Ion-beam irradiation of DLC-based nanocomposite: creation of a highly biocompatible surface, Appl. Surf. Sci. 469 (2019) 896–903.
[69] J. Xu, K. Lu, D. Fan, Y. Wang, S. Xu, M. Kubo, Different etching mechanisms of diamond by oxygen and hydrogen plasma: a reactive molecular dynamics study, J. Phys. Chem. C 125 (30) (2021) 16711–16718.
[70] A.R. Shahmoradi, M.S. Bejandi, E.H. Rasanani, A.A. Javidparvar, B. Ramezanzadeh, Graphene oxide nano-layers functionalized/reduced by L-Citrulline/Pectin bio-molecules for epoxy nanocomposite coating mechanical properties reinforcement, Prog. Org. Coating 178 (2023) 107493.
[71] K. Li, G. Xu, X. Wen, J. Zhou, F. Gong, High-temperature friction behavior of amorphous carbon coating in glass molding process, Friction 9 (6) (2020) 1648–1659.
[72] A. Erdemir, C. Donnet, Tribology of diamond-like carbon films: recent progress and future prospects, J. Phys. Appl. Phys. 39 (18) (2006) 311–327.
[73] C. Yang, Z.M. Sun, C.Y. Wang, A.H. Huang, T. Ying, L.P. Zhou, Z.S. Ye, S. Xiao, P. K. Chu, X.Q. Zeng, A self-sealing and self-healing MAO corrosion-resistant coating on aluminum alloy by in situ growth of CePO4/Al2O3, Corros. Sci. 245 (2025) 112706.

Supplementary Material

Evolution and Mechanism of Frictional Properties of DLC Coatings and Iron Surfaces under Hydrogen-Atom Irradiation

Hu Zhang[a], Shu Xiao[a, *], Yong Huang[a], Qingdong Ruan[a], Guohua Chen[a], Saihua Jiang[a], Chao Yang[b, *], Paul K. Chu[c]

[a] School of Mechanical & Automotive Engineering, South China University of Technology, Guangzhou 510641, China

[b] National Engineering Research Center of Light Alloy Net Forming, School of Materials Science and Engineering, Shanghai Jiao Tong University, Shanghai 200240, China

[c] Department of Physics, Department of Materials Science and Engineering, and Department of Biomedical Engineering, City University of Hong Kong, Tat Chee Avenue, Kowloon, Hong Kong, China

[*] Corresponding authors: xiaos@scut.edu.cn (S. Xiao), chaoyang0315@163.com (C. Yang)

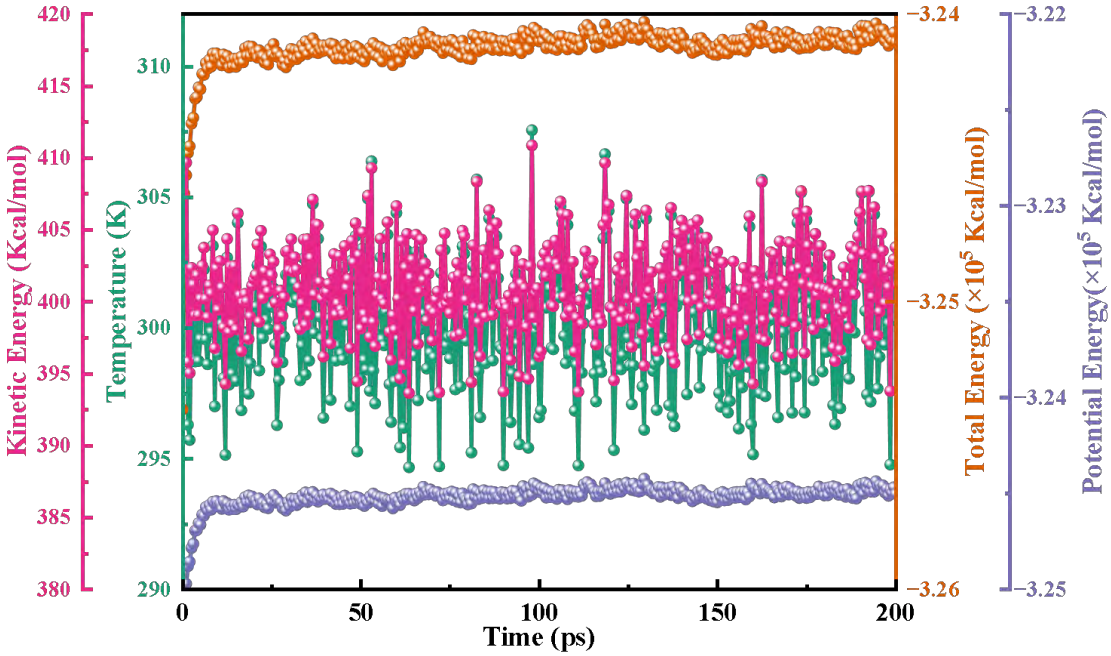

Fig. S1. Time-dependent evolution of kinetic energy, potential energy, total energy, and interfacial temperature during hydrogen irradiation.

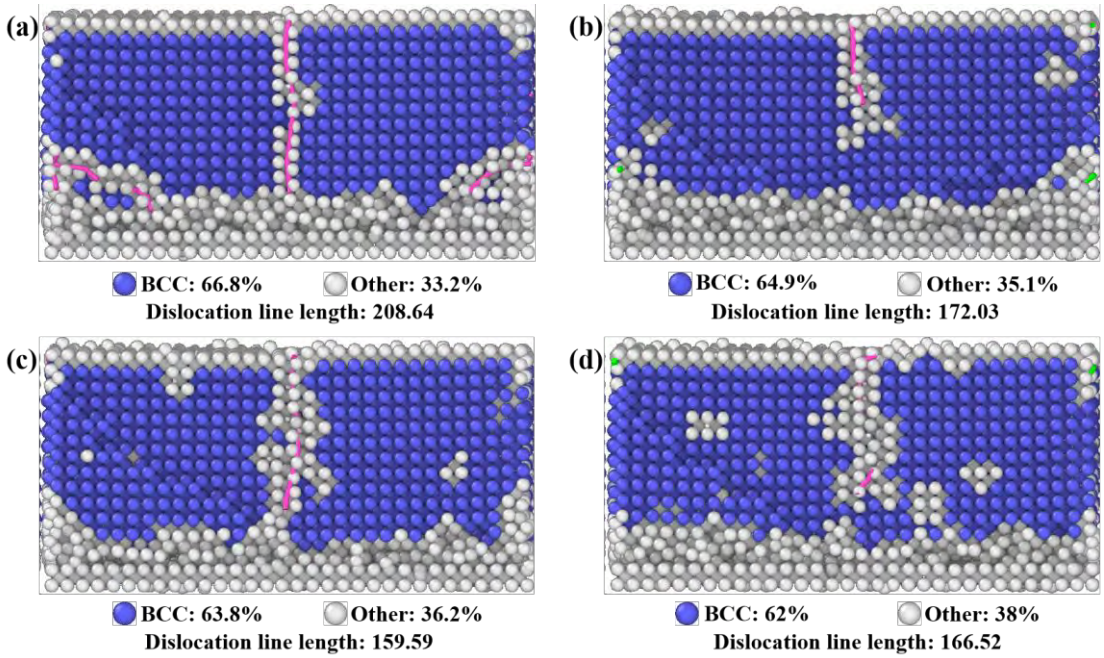

Fig. S2. The dependence of atomic structure and dislocation evolution on the irradiation dose of hydrogen atoms in Fe matrix: (a) 50 hydrogen atoms, (b) 100

hydrogen atoms, (c) 150 hydrogen atoms, (d) 200 hydrogen atoms.

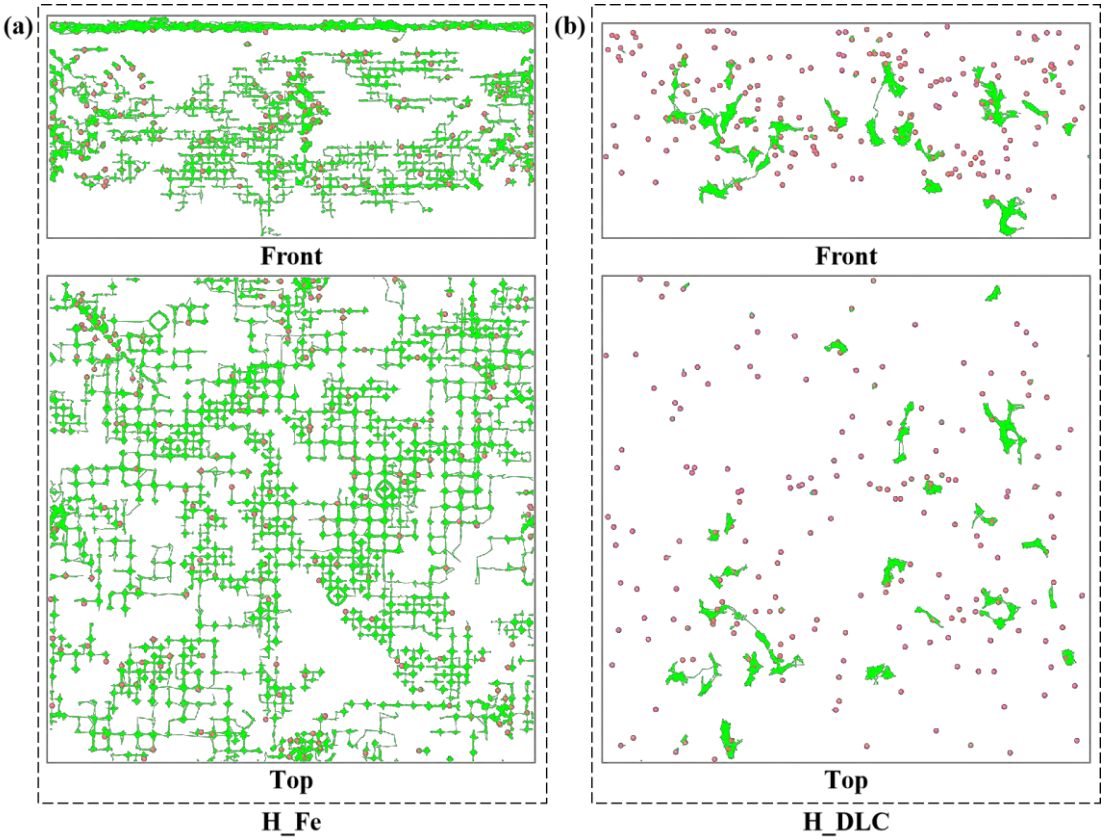

Fig. S3. The distribution and trajectory of hydrogen atoms: disregard of the morphology of DLC and Fe. (The green line represents the trajectory of the atom, and the red sphere represents the H atom.)

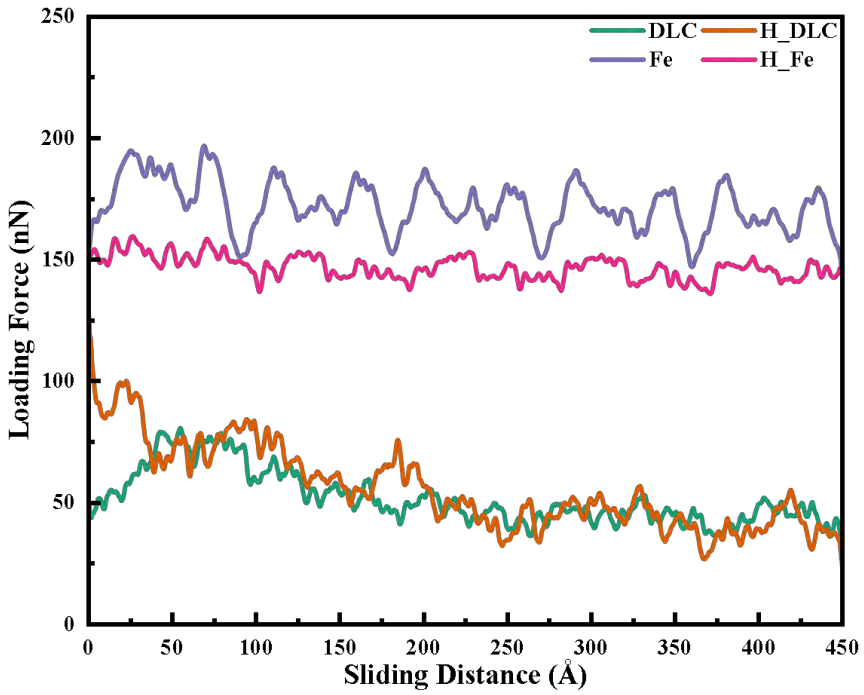

Fig. S4. The load variation during friction

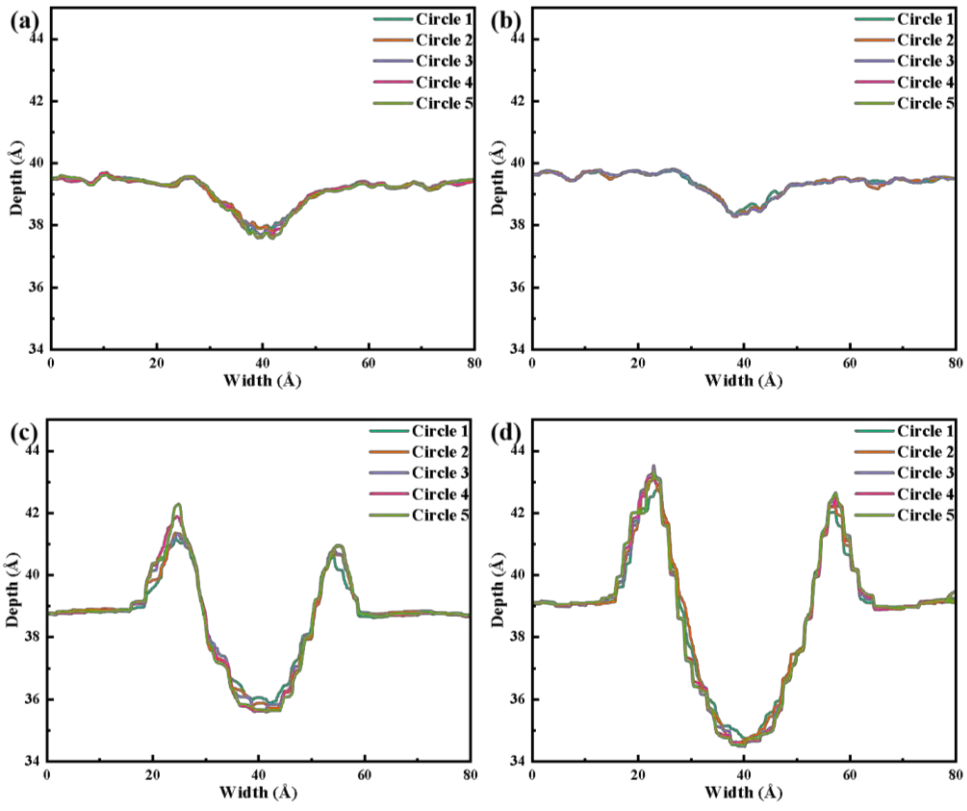

Fig. S5. Analysis of cross-sectional wear scar morphology between non-irradiated

system and h-atom irradiation system: (a) unirradiated DLC coating, (b) H-atom irradiated DLC coating, (c) unirradiated Fe substrate, (d) H-atom irradiated Fe substrate.

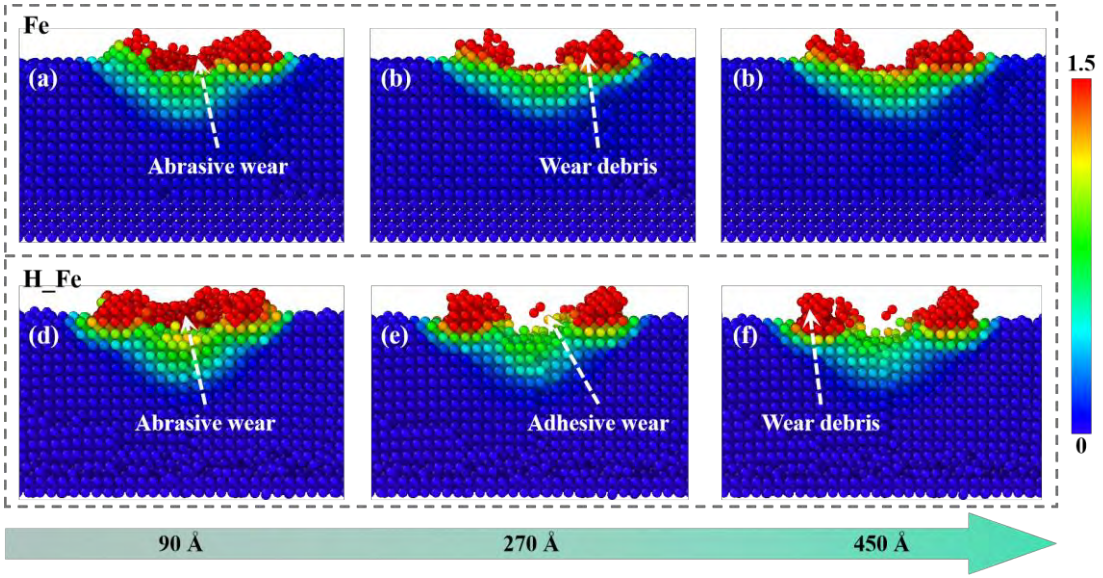

Fig. S6. The left view of the surface shear strain of unirradiated (Fe) and H-atom irradiated (H_Fe) Fe substrates.

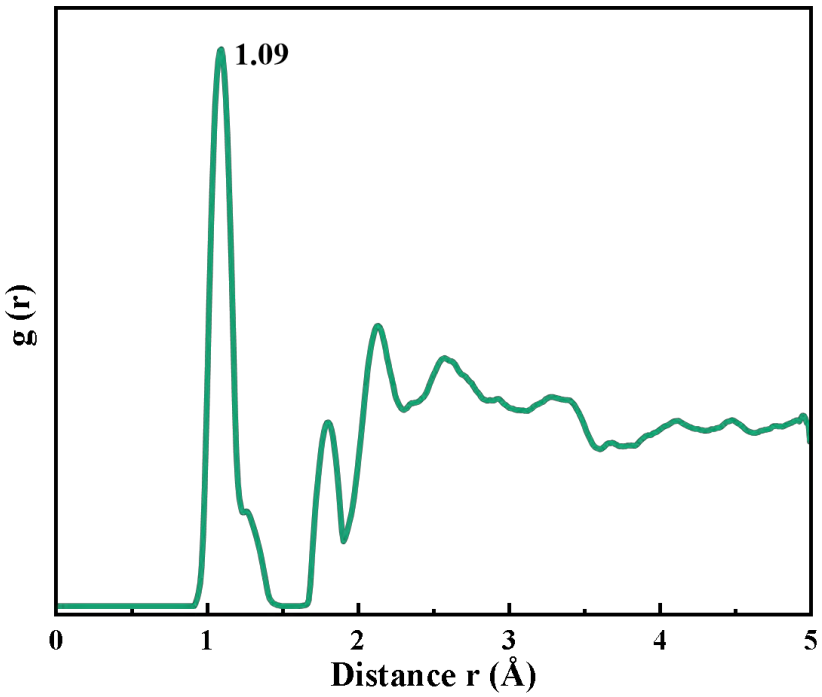

Fig. S7. Radial distribution function for C-H.

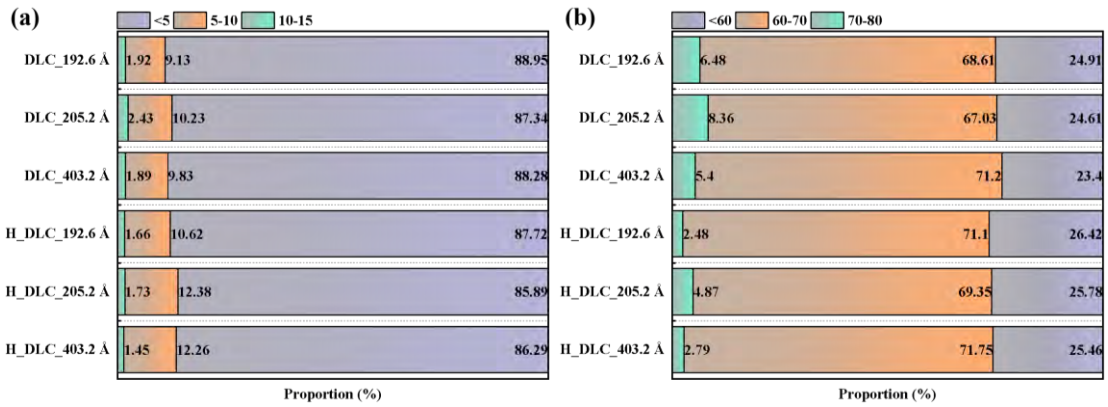

Fig. S8. Stacking bar chart of the interface stress distribution ratio, (a) Hydrostatic stress, (b) Von Mises stress

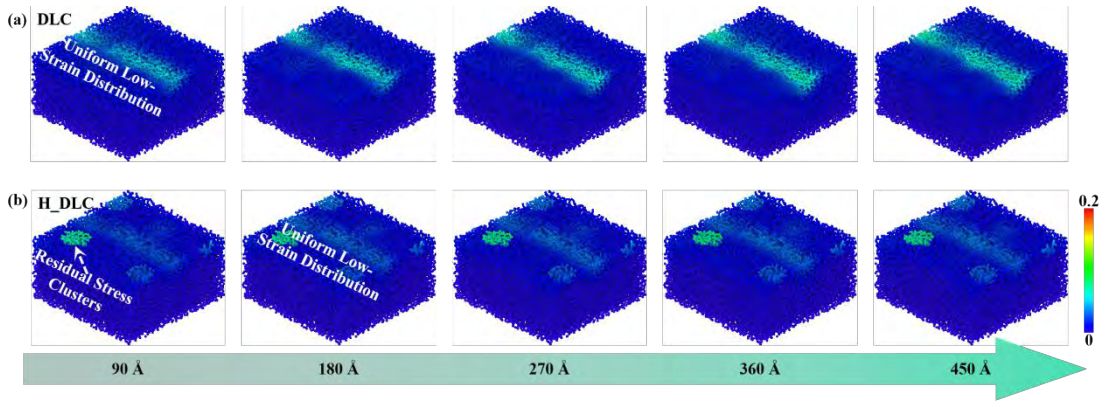

Fig. S9. Presents an analysis of stress strain variation with sliding distance in both unirradiated (DLC) and hydrogen-atom irradiated (H_DLC) DLC coatings: (a) unirradiated DLC coating, (b) H-atom irradiated DLC coating.

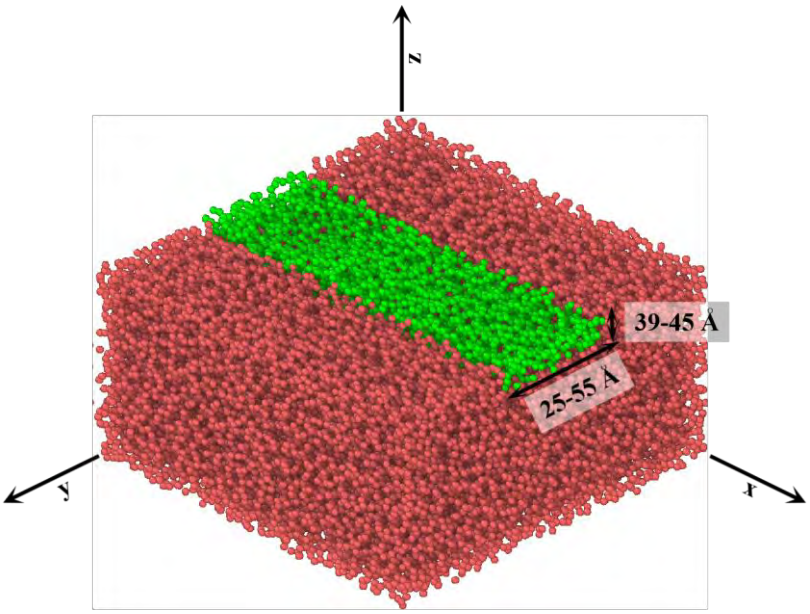

Fig. S10. Data extraction model for quantifying the variation of hybrid bond content within the wear scar interface, with green atoms representing the computational domain.

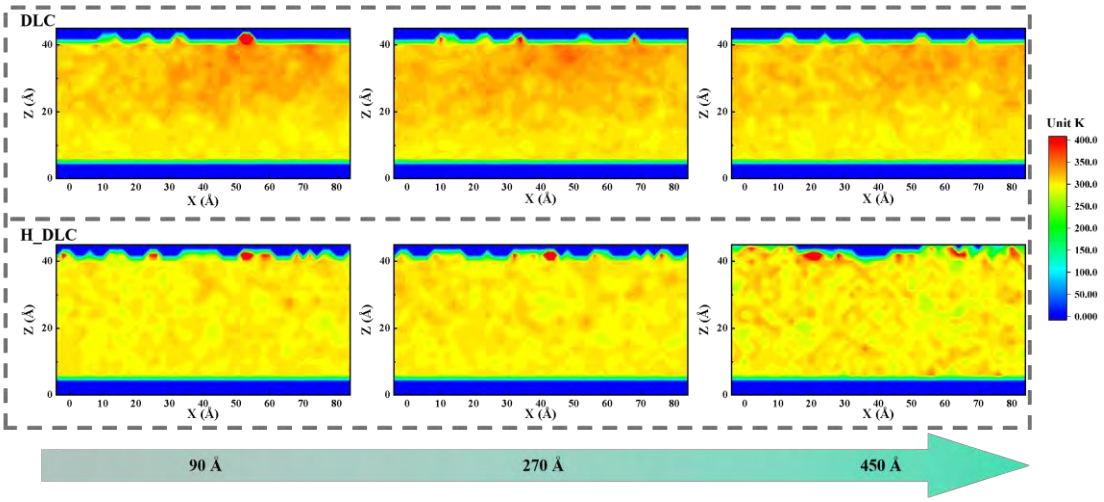

Fig. S11. Spatial temperature distribution profile at the frictional contact zone.

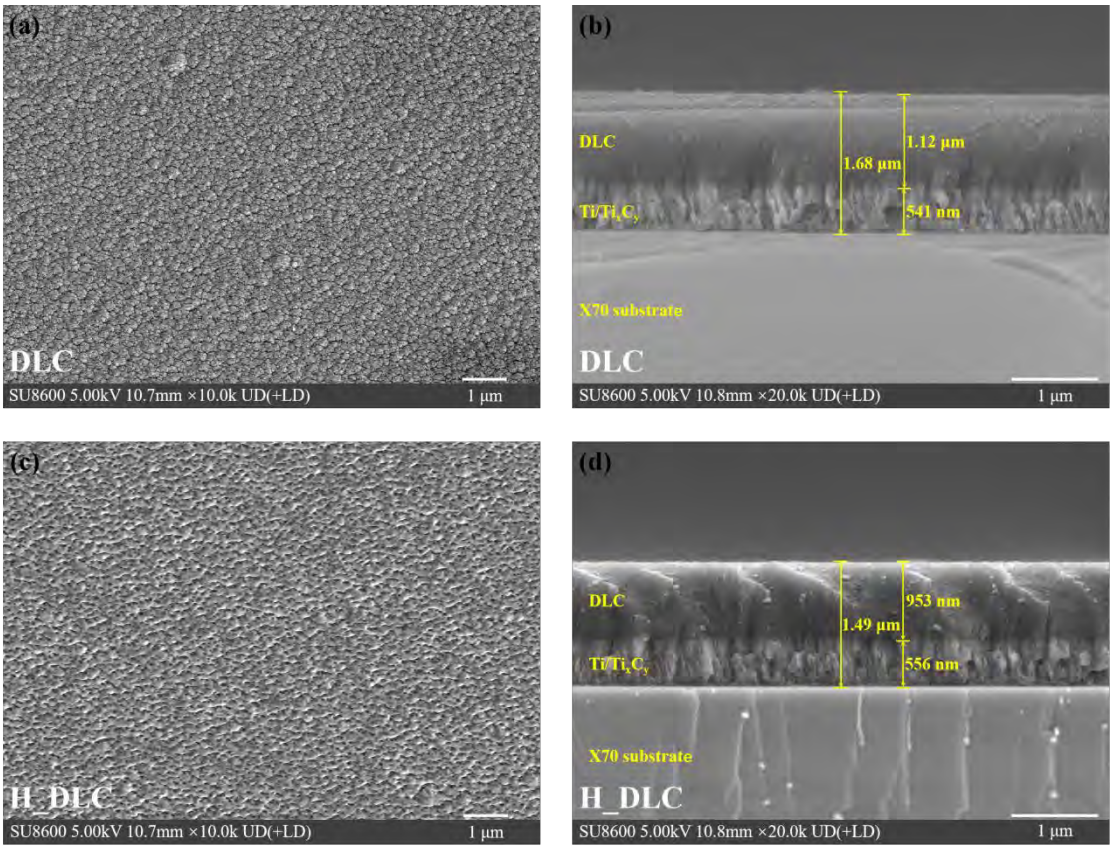

Fig. S12: The surface and cross-sectional morphologies of unirradiated DLC coatings (a-b) and H-atom-irradiated DLC coatings (c-d) were characterised using field

emission scanning electron microscopy.

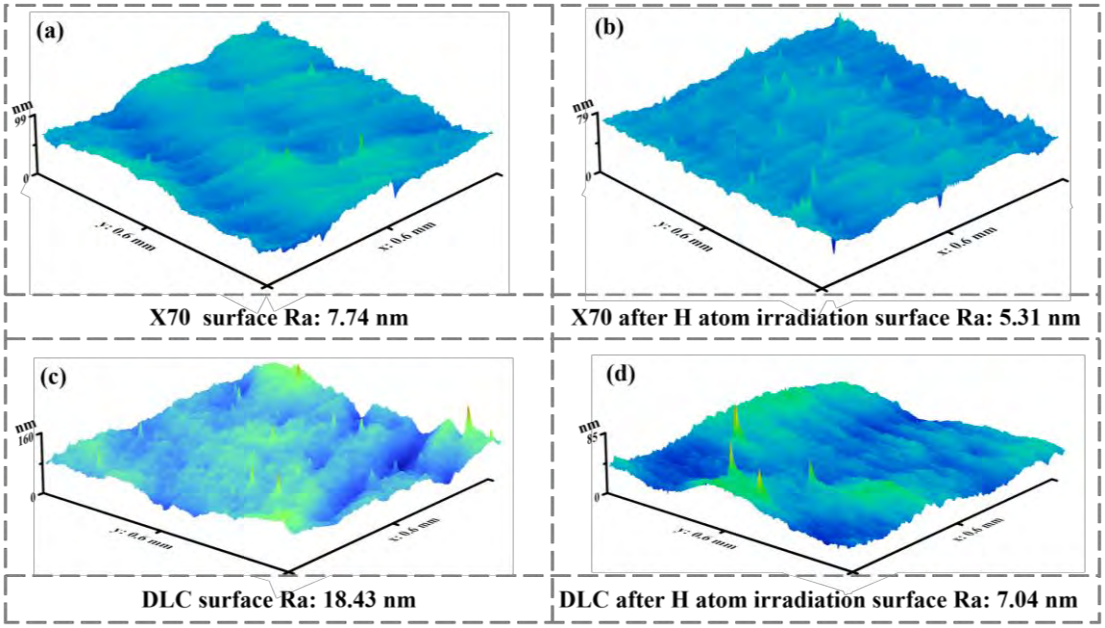

Fig. S13. Surface topography characterization of unirradiated and H-atom irradiated samples using optical profilometry: (a) unirradiated Fe substrate, (b) H-atom irradiated Fe substrate, (c) unirradiated DLC coating, (d) H-atom irradiated DLC coating.

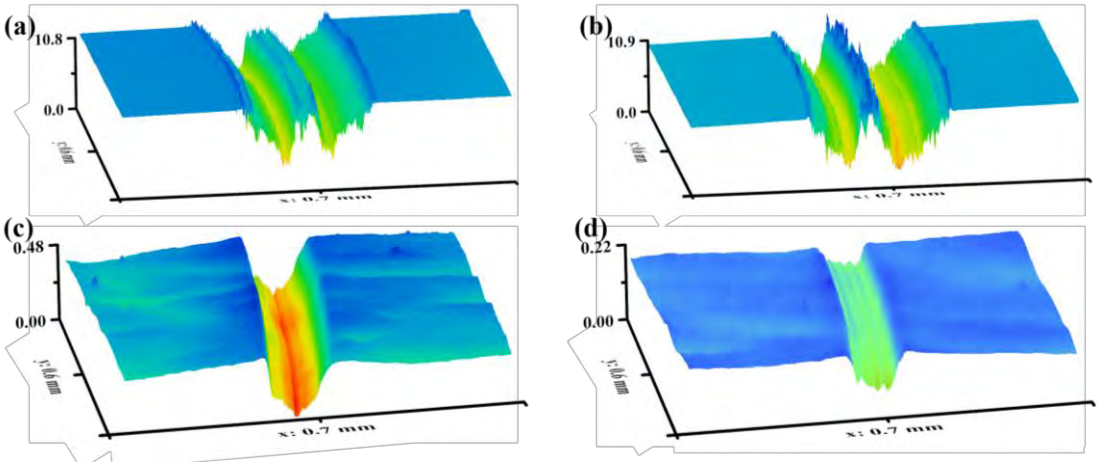

Fig. S14. Wear scar morphology analysis of unirradiated and H-atom irradiated samples using optical profilometry: (a) unirradiated Fe substrate, (b) H-atom irradiated Fe substrate, (c) unirradiated DLC coating, (d) H-atom irradiated DLC coating.

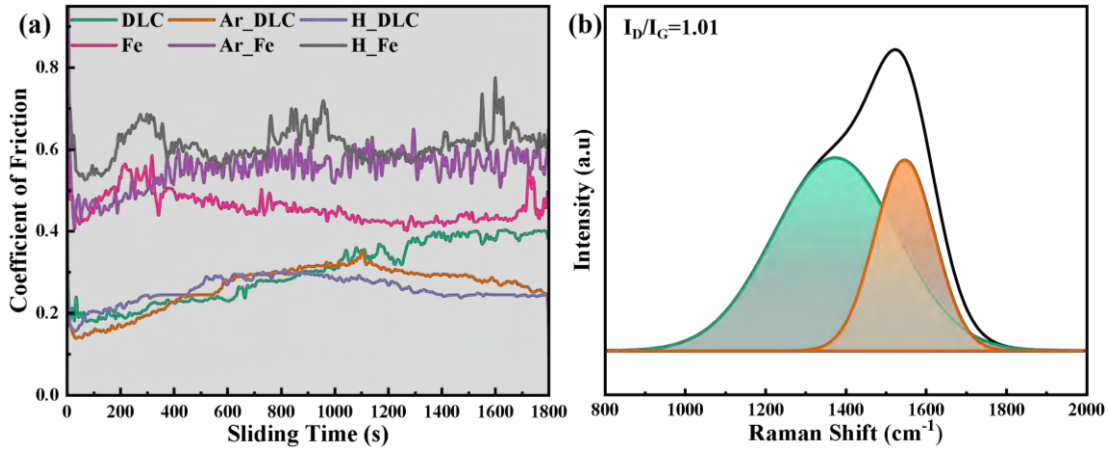

Fig. S15. (a) Friction coefficient profiles of specimens treated in pure Ar versus Ar-hydrogen mixed plasma environments; (b) Raman spectra of pure Ar-atom irradiated DLC coating surface.